Marine Micropaleontology 176 (2022) 102160

Contents lists available at ScienceDirect

Marine Micropaleontology

journal homepage: www.elsevier.com/locate/marmicro

Reflooding and repopulation of the Mediterranean Sea after the Messinian Salinity Crisis: Benthic foraminifera assemblages and stable isotopes of Spanish basins

F. Bulian [a,e,*], T.J. Kouwenhoven [b], N. Andersen [c], W. Krijgsman [d], F.J. Sierro [a]

[a] Dept. de Geología, Univ. de Salamanca, Plaza de los Caídos s/n, 37008 Salamanca, Spain
[b] Faculty of Earth Sciences, Utrecht University, Utrecht, the Netherlands
[c] Leibniz-Laboratory for Radiometric Dating and Isotope Research, Christian-Albrechts-Universität Kiel, Max-Eyth-Str.11-13, 24118 Kiel, Germany
[d] Palaeomagnetic Laboratory Fort Hoofddijk, Utrecht University, Budapestlaan 17, 3584 CD Utrecht, the Netherlands
[e] Groningen Institute of Archeology, University of Groningen, Poststraat 6, 9712 ER Groningen, the Netherlands

ARTICLE INFO

Keywords:
Miocene-Pliocene boundary
Alboran Basin
Spanish marginal basins
Benthic foraminifera

ABSTRACT

Benthic foraminiferal, sedimentological, and stable isotope analyses performed on early Zanclean sediments from Alboran Basin ODP Site 976 and southern Spanish land-based sections in the Malaga, Nijar and Sorbas basins have enabled the reconstruction of Mediterranean environmental conditions immediately after the Messinian Salinity Crisis. The presence at the Miocene – Pliocene boundary of dark layers, often enriched in organic matter, suggests that the Zanclean reflooding has created water column stratification, and reduced bottom-water oxygen levels. Considering that such dark layers are recorded at both deep and marginal settings far away from the Gibraltar gateway/s, a Mediterranean-scale water-mass stratification must have occurred. This stratification could be the result of saline Atlantic waters sinking into a less saline Mediterranean Basin still under the influence of the Paratethys. Our early Zanclean benthic $\delta^{18}O$ data show that the Mediterranean water budget was indeed less negative than at present, explaining the lower salinity of the basin. However, the Atlantic values of the benthic $\delta^{13}C$ registered in the Alboran basin suggest that bottom-water renewal rates were quite high during the early Zanclean, preventing the reduction of $\delta^{13}C$ at the seafloor as observed in the Messinian records. Zanclean benthic foraminiferal repopulation sequences show similarities with recovery from low-oxic episodes during sapropel deposition. These observations, paired with the gradual deepening of the basins, suggests that the Zanclean reflooding led to a progressive shift from stressed and unstable environments towards benthic associations typical of efficient circulation and bottom water ventilation.

1. Introduction

Since the 1970s there is an ongoing debate regarding the end of the Messinian Salinity Crisis (MSC) of the Mediterranean Sea (Fig. 1A) and the exact dynamics of restoration of marine conditions. Through time three main reflooding scenarios were proposed: (1) an instantaneous inundation of an (almost) desiccated Mediterranean at 5.33 Ma, corresponding to the base of the Zanclean (Hsü, 1972; Blanc, 2002; Loget and Van Den Driessche, 2006; Garcia-Castellanos et al., 2009; García-Alix et al., 2016); (2) high Mediterranean water level during the latest Messinian with rapid restoration of the Atlantic-Mediterranean connection characterised by a minor sea-level rise across the Messinian-Zanclean transition (Loget et al., 2005; Pierre et al., 2006; Roveri and Manzi, 2006; Cornée et al., 2016; Marzocchi et al., 2016; Andreetto et al., 2021b) and (3) a two-stage restoration of the connection with the major reflooding taking place at 5.46 Ma, during the Messinian (Estrada et al., 2011; Bache et al., 2012; Pérez-Asensio et al., 2013; Bache et al., 2015). The three models differ not only in the dynamics of the reflooding itself, but also in the timing and the magnitude of the base level fluctuations.

The Zanclean sediments in the Mediterranean were deposited on top of shallow (Nijar Basin: Bassetti et al., 2006, this work; Malaga Basin: Guerra-Merchán et al., 2008, this work; Sorbas Basin, this work; Fig. 1B) and deep, late Messinian Lago-Mare (LM) deposits (Eraclea Minoa: e.g.,

* Corresponding author at: Dept. de Geología, Univ. de Salamanca, Plaza de los Caídos s/n, 37008 Salamanca, Spain.
E-mail addresses: fra.bulian@usal.es (F. Bulian), T.J.Kouwenhoven@uu.nl (T.J. Kouwenhoven), nandersen@leibniz.uni-kiel.de (N. Andersen), W.Krijgsman@uu.nl (W. Krijgsman), sierro@usal.es (F.J. Sierro).

https://doi.org/10.1016/j.marmicro.2022.102160
Received 9 March 2022; Received in revised form 6 August 2022; Accepted 9 August 2022
Available online 16 August 2022

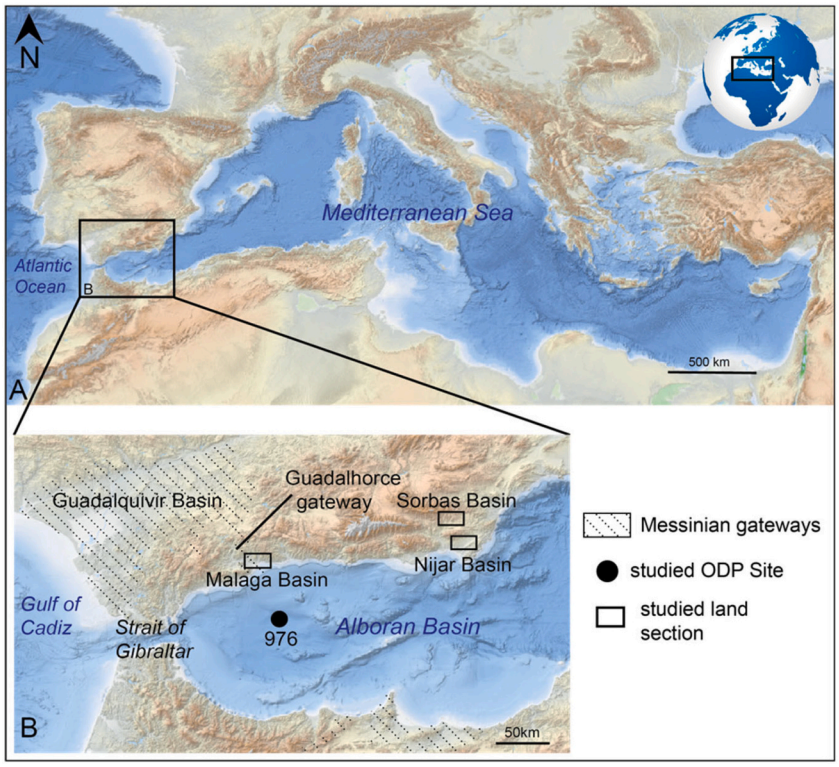

Fig. 1. A) Bathymetric map of the Mediterranean region (from https://portal.emodnet-bathymetry.eu/) where the rectangle shows the studied area and the Guadalquivir Basin. B) Bathymetric map of the Alboran Basin and Rifian Corridor. The black dot and rectangles indicate the studied ODP Site and onshore sections (Rio Mendelin section-Malaga basin; Zorreras section-Sorbas Basin and Barranco del Negro section-Nijar Basin) respectively. The hatched areas show the extension of the Messinian gateways (after Martín et al., 2014).

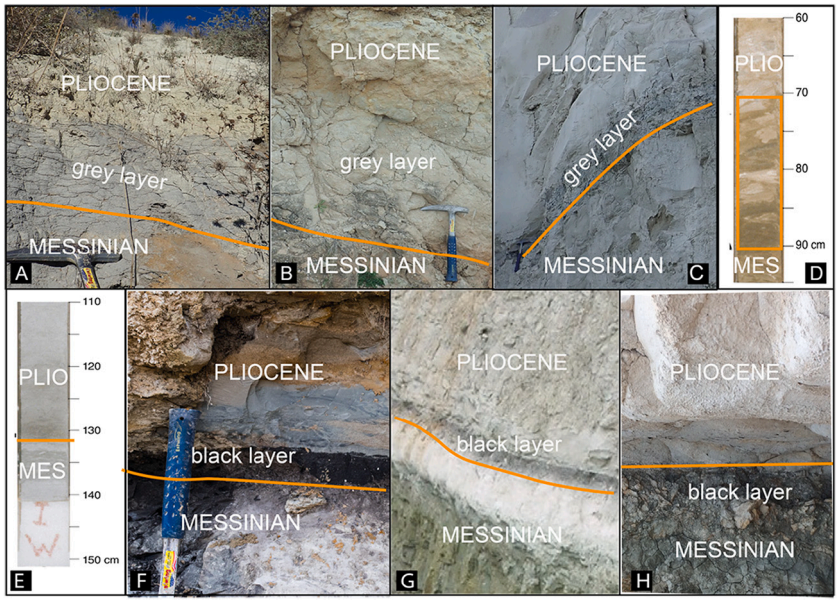

Fig. 2. Photographs of the Miocene-Pliocene boundary from some of the mentioned locations. A) Rio Mendelin section (this study); B) Zorreras section (this study); C) Eraclea Minoa section (personal collection); D) ODP Site 974 (Iaccarino et al., 1999b); E) ODP Site 975 (Iaccarino et al., 1999b); F) Barranco del Negro section (this study); G) Moncucco quarry in Piedmont Basin (courtesy of. F. Andreetto) and H) Zakynthos island in Greece (courtesy of K. Agiadi).

Brolsma, 1978; Sites 975 and 974: Iaccarino and Bossio, 1999; Iaccarino et al., 1999a). The contact at the Miocene-Pliocene boundary (MPB) is expressed in different ways including conformably above continental facies (Sorbas Basin, e.g., Roveri et al., 2018), and erosional both in deep and shallow basins (e.g., Chelif Basin: Rouchy et al., 2007; Zakynthos Island: Kontakiotis et al., 2016 and Karakitsios et al., 2017; Vera Basin: Caruso et al., 2020; Alboran Basin: Bulian et al., 2021). At some locations conglomerates, breccias or small clasts are intercalated (Site 975: Iaccarino et al., 1999b (Fig. 1E); East Alboran Basin: Garcia-Castellanos et al., 2019; Levant Basin: Madof et al., 2019). In land sections and offshore sites, the boundary is recognized through changes in lithology, carbonate content or stable isotopes of carbonates (Iaccarino et al., 1999b; Pierre et al., 2006; Rouchy et al., 2007).

A characteristic lithology identified at the MPB (marking the earliest Pliocene sediments and/or latest Messinian ones) is a cm/dm-thick black layer deposited conformably above the LM deposits in the Piedmont Basin (Fig. 2G; Trenkwalder et al., 2008; Dela Pierre et al., 2016), Northern Apennines (Northern Apennine; Gennari et al., 2008; Grossi

Fig. 3. Field photograph of the Miocene-Pliocene boundary in the Malaga Basin (Rio Mendelin section).

et al., 2008), Northern Italy (Riforgiato et al., 2011), Cyprus (Rouchy et al., 2001; Manzi et al., 2016), Sicily (Brolsma, 1978; unpublished data; Fig. 2C), DSDP Site 376 (Cita et al., 1978), ODP Sites 974 and 975 (Iaccarino et al., 1999b; Fig. 2D, E), Zakynthos (Fig. 2H; K. Agiadi, pers. comm.) and in sections in the Malaga, Sorbas and Nijar Basins included in this study (Fig. 2A, B, F). At some locations (e.g., Malaga Basin) these layers are deposited just above the MPB. This black layer is usually rich in organic matter (Gennari et al., 2008; Trenkwalder et al., 2008; Manzi et al., 2016) and scarce in foraminifera which are usually typical Pliocene species, reworked Miocene to Eocene species, or in some cases both (Cita and Zocchi, 1978; Gennari et al., 2008; Manzi et al., 2016). At some locations microfossils are absent (e.g. Moncucco quarry: Trenkwalder et al., 2008). The palaeoenvironmental significance of such dark layers remains still largely unknown (e.g. Gennari et al., 2008).

To test and validate the most probable reflooding scenario and explain the occurrence of dark layers it is necessary to increase our understanding of the palaeoenvironmental conditions present after the MSC and therefore, to analyse the late Messinian - early Zanclean sedimentary record at locations close to the Mediterranean – Atlantic gateway. In this work, we studied three onshore outcrops from Neogene basins in southern Spain which contain well-preserved late Miocene – early Pliocene sedimentary successions: the Rio Mendelin section in the Malaga Basin, the Barranco del Negro section in the Nijar Basin and the Zorreras section in the Sorbas Basin (Fig. 1B). In addition, we re-evaluated the early Zanclean sediments retrieved at ODP Site 976 in the West Alboran Basin, located in front of the Gibraltar gateway (Fig. 1B). During the late Miocene, these basins were part of the Mediterranean realm and consequently their sediments could have registered the first influx of Atlantic waters, together with Zanclean water levels and palaeoenvironmental conditions in the western Mediterranean. We performed detailed benthic foraminiferal and stable isotope analyses of these four sites to better understand the dynamics of the reflooding together with the environmental changes that occurred in the Mediterranean after the MSC.

2. Geological setting and material studied

2.1. Neogene Basins of the Betic Cordillera

The Malaga Basin (Fig. 1B) is an intermontane *E*-W oriented basin located in the westernmost sector of the Betic Cordillera (Sanz De Galdeano and Vera, 1992). The basin is drained by the Guadalhorce River and bounded to the north by the Malaga Mountains, to the south by the Mijas Sierra and to the east by the Alboran Basin. Its post-orogenic infilling is composed of upper Tortonian to Quaternary sediments (e.g. Guerra-Merchán et al., 2008). The section analysed in this study (Rio

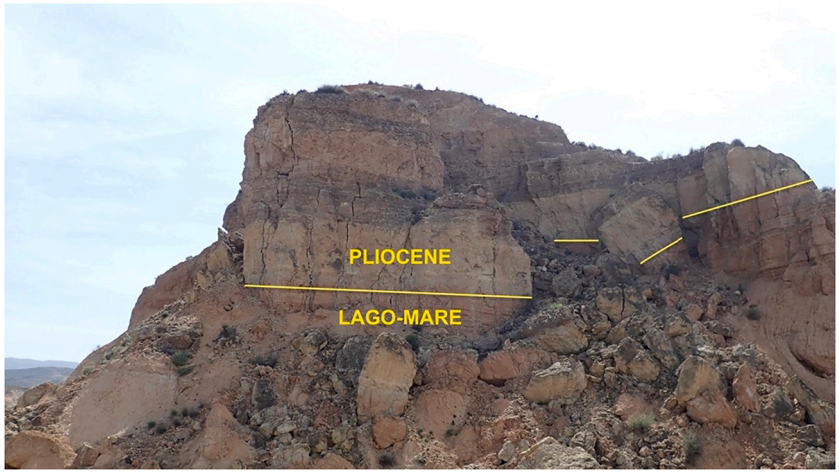

Fig. 4. Field photograph of the Miocene-Pliocene boundary in the Sorbas Basin (Zorreras section).

Fig. 5. Field photograph of the Miocene-Pliocene boundary in the Nijar Basin (Barranco del Negro section).

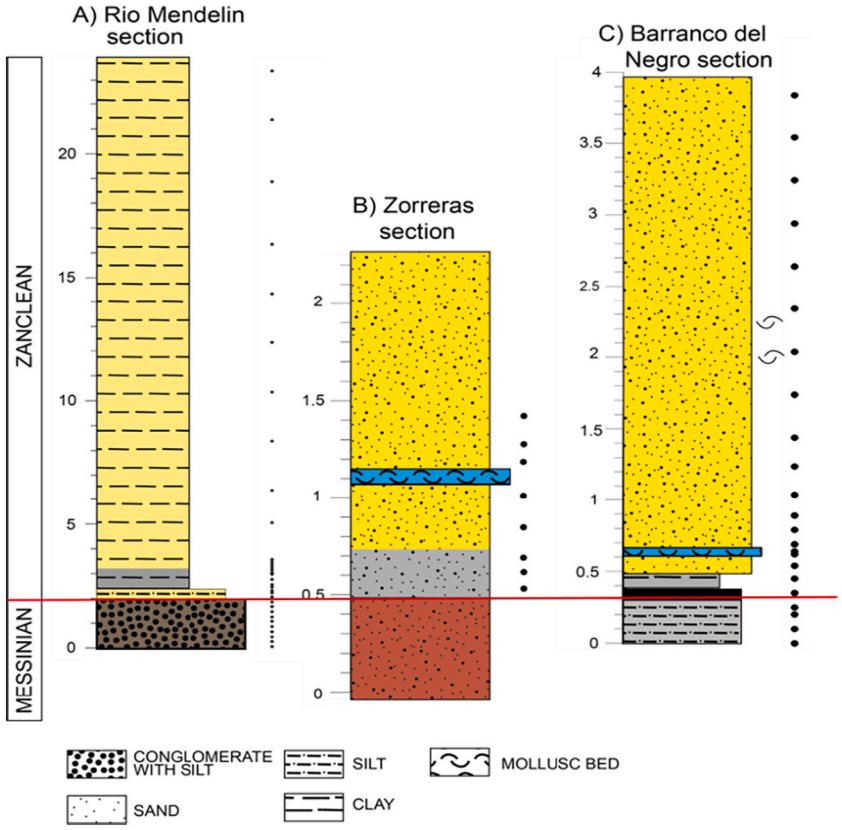

Fig. 6. Stratigraphic logs of the three sections studied in Southern Spain. A) Rio Mendelin section; B) Zorreras section, C) Barranco del Negro section. The black dots represent the analysed samples. The colours reflect the colours observed in the field.

Mendelín section; 36°45′2.53”N; 4°25′57.26”W; Fig. 2A, 3, 6A) comprises late Messinian deposits related to the final stage of the MSC (Lago-Mare unit) and the lower Zanclean. The Río Mendelín section is located in an ancient fluvial valley, incised during the latest Tortonian or during the MSC acme sea level drop, which, based on the Paratethyan affinity of its faunal content, was progressively refilled during the dilution phase at the end of the Messinian (Guerra-Merchán et al., 2010; Do Couto et al., 2014). The Pliocene sediments are deposited with an erosional contact at the margins and a gradual conformable contact in the centre of the basin on top of the LM unit. In this study, we analysed 23.5 m of the Rio Mendelin section, including 2 uppermost metres of the LM sequence followed, with a transitional contact, by early Pliocene sediments composed of 25 cm of yellow silty sediments, 75 cm of grey clays overlain by 20.5 m of yellowish clays (Fig. 6A).

The Nijar and Sorbas basins are intermontane basins developed above the metamorphic nappes of the southern Betics (Fig. 1; Sanz De Galdeano and Vera, 1992). The sedimentary infilling of the basins occurred during the late Miocene (Tortonian and Messinian), Pliocene and Quaternary (Dabrio et al., 1981; Serrano, 1990; Omodeo Salé et al., 2012). During the Miocene, until the end of MSC Stage 1, the two basins

were connected to the Mediterranean, which entered the Nijar Basin from the south and the Sorbas Basin through NW-SE trending corridors north of Nijar (Fortuin and Krijgsman, 2003).

In this work, the upper Messinian-lower Zanclean sediments from the Nijar and Sorbas basins have been studied (Figs. 4 and 5). In the Sorbas Basin, lower Pliocene sediments (Gochar Formation) lie on top of the Zorreras Member which mainly consists of palaeosols, fluvio-deltaic reddish silts and sandstones, grey-coloured sandstones and conglomerates intercalated by up to 4 whitish, massive carbonate beds (Manzi and Roveri, 2009; Aufgebauer and McCann, 2011; Roveri et al., 2018; Roveri et al., 2019b) containing euryhaline ostracod specimens of Paratethyan affinity like *Cyprideis* sp. (e.g., Aufgebauer and McCann, 2011). The Zorreras member is considered as the equivalent of the LM facies (Rouchy and Caruso, 2006). The marine early Pliocene sands show 0.5 m above the boundary a fossiliferous horizon rich in bivalves (Fig. 6B) that can be traced throughout the basin (Mather and Stokes, 2001; Roveri et al., 2019b). Here, we analysed 2 m of the Zorreras section (37° 6′ 9.87″ N; 2° 6' 46.78″ W) composed of 0.5 m of reddish LM deposits, 0.3 m of grey deposits containing carbonate nodules and 1.2 m of Zanclean massive sands including the intercalated bivalve horizon (Fig. 4 and 6B).

In the Nijar Basin (Fig. 1B), the upper Messinian is composed of alternations of marly LM facies and conglomerate alluvial beds (Omodeo Salé et al., 2012) of the Feos Formation, which are overlain by the lowermost Zanclean with an unconformity in the marginal parts of the basin and a conformable contact at the centre (Fortuin and Krijgsman, 2003; Aguirre and Sánchez-Almazo, 2004; Roveri et al., 2019a). This study focuses on the Barranco del Negro section (Fig. 2F, 5, 6C; 37° 0′ 35.02″ N; 1° 58' 23.02″ W) in the north-eastern part of the Nijar Basin. Here, the MPB can be clearly identified, with a sharp contact over uppermost Messinian sediments, a 5 cm-thick black and 5 cm-thick grey layer topped by lower Zanclean massive yellow bioclastic marine sands, characterised at the base by a 1 cm-thick layer with bivalve shell fragments (Fig. 2F, 6C).

2.2. Alboran Basin

The Alboran Basin is a transitional area between the semi-enclosed Mediterranean Sea and the Atlantic Ocean (Fig. 1A, B) characterised by vigorous circulation that is strongly related with water exchange at the Gibraltar Strait where the relatively low-salinity Atlantic waters enter the Mediterranean on top of high-salinity Mediterranean water masses.

ODP Site 976 (36° 12′ 18.78" N, 4° 18′ 45.78" W) is located in the northern sector of the West Alboran Basin (WAB; Western Mediterranean), ~100 km to the east of the Gibraltar Strait on top of a continental crustal horst that formed during early- to mid-Miocene rifting (Comas et al., 1996). The marine lower Pliocene sediments recovered at this site are mainly composed of homogeneous nannofossil-rich claystone and sandy claystone (Comas et al., 1996) with no visible changes in colour. We analysed 32 samples from the lower Pliocene of core 61. From the underlying core 62, only section 62×-CC was recovered in which three samples were collected. Because of their uncertain stratigraphic position, these have been excluded from the micropaleontological interpretation (Bulian et al., 2021). The position of the MPB was previously estimated with the aid of seismic interpretation and regional biostratigraphy at the base of core 61 (Bulian et al., 2021), corresponding with a visible erosional surface. This erosion has been associated with the Zanclean reflooding, when after the breaching of the Gibraltar Strait, the Atlantic water would have abruptly entered the Mediterranean (Garcia-Castellanos et al., 2009; Estrada et al., 2011) and produced a marked incision (Esteras et al., 2000; Blanc, 2002). Alternatively, if a modest drawdown is considered, a hyperpycnal submarine cascading erosion (Roveri et al., 2014b) could be the creation mechanism. The time slice represented by the hiatus has been estimated at 1.67 Ma and includes the majority of the middle-upper Messinian sediments (Bulian et al., 2021).

3. Methodology

3.1. Micropalaeontological analyses

For this study, a total of 95 samples (33 from the Rio Mendelin section, 32 from ODP Site 976, 21 from the Barranco del Negro section, 9 from the Zorreras section) taken with variable sampling steps (10–20 cm for the Barranco del Negro and, Zorreras sections and Site 976 and between 10 cm and 1 m for the Rio Mendelin section) were selected for micropalaeontological analyses. The samples were oven dried at 40 °C and washed over 63 μm and 150 μm sieves. For faunal analysis, aliquots of the 150 μm fraction of on average 150–200 benthic foraminifera were counted. The counts of benthic foraminifera were then transferred to relative frequencies. Samples yielding <50 specimens were not included in the analyses and interpretations. The benthic foraminiferal content of the Zorreras section has been studied in a semi-quantitative way based on the presence or absence of species considering that very few specimens were present. Similarly, in the three land-based sections the presence of ostracods was recorded, but only the LM marker species (*Cyprideis* sp.) was identified from the assemblage.

The diversity of the benthic foraminiferal assemblages has been estimated through the Shannon index (H, Murray, 1991; Spellerberg and Fedor, 2003), expressed by the formula:

$$H = -K\sum_{i=1}^{n} piln(pi)$$

where *pi* is the proportion of the i^{th} species and K a positive constant.

For ODP Site 976, of which the Messinian part was deposited at slope depth (Bulian et al., 2021) the sum of shallow-water benthic foraminiferal species, *Elphidium* spp., *Rosalina* spp., discorbids and *Cibicides lobatulus* (Supp. 1) was calculated. Because a relatively high number of displaced specimens indicates downslope transport (Fentimen et al., 2020 and references therein) this sum has been used as an indicator of currents in the basin.

3.2. Statistical analyses

Of each data set except from the Zorreras and Barranco del Negro sections (Supp. 2), a hierarchical cluster analyses (Pearson correlation: Past 4.02 software; Hammer et al., 2001; Hammer et al., 2008) was performed on the most abundant (≥ 3%) variables (taxa) to identify the distributional patterns of benthic foraminiferal species assemblages occurring in similar environments. Species with rare or single occurrences were removed from the data whereas species belonging to the same genus, when considered indicative of analogous environmental conditions, were grouped together. *Nodosaria* spp. comprises unilocular spp., *Nodosaria* spp., *Pseudonodosaria* spp., *Lagena* spp. and *Procerolagena* spp., *Cancris* spp. contains the species *C. oblongus* and *C. auriculus*. *Uvigerina peregrina* includes both *Uvigerina peregrina* and *U. pygmea*, and *Bulimina striata* is the sum of *B. striata* and *B. striata mexicana*. In *Pullenia quinqueloba*, both forms with four and five chambers were included.

3.3. Palaeo – water depth estimates

Palaeo-water depth estimates were initially performed using the ratio (P/(P + B))*100 (%P; Gibson, 1989; Van der Zwaan et al., 1990), which, although this reflects general sea-level trends, has disadvantages related to sensitivity to oxygen levels, food availability and preferential dissolution of the planktic fauna (e.g., Sen Gupta and Machain-Castillo, 1993; Jorissen et al., 1995; Kucera, 2007). To improve the reliability of palaeodepth estimations, we excluded from the ratio the infaunal foraminiferal species (e.g., buliminids, bolivinids, uvigerinids, *Nonion* spp.). This forms the basis for calculation of the regression function (Van der Zwaan et al., 1999; Van Hinsbergen et al., 2005). However, this approach still does not account for dissolution of planktic foraminifera.

Table 1
The bathymetric ranges, mean living depth and standard deviation of the benthic foraminiferal species used for palaeo – water depth reconstruction. The species used for the Rio Mendelin section are underlined, while the ones employed for ODP Site 976 have an asterisk. Depth ranges are based on previously published work of: 1 Wright (1979), 2 Wright (1978), 3 Lutze and Coulbourn (1984), 4 Pflum et al. (1976), 5 Lutze and Wefer (1980), 6 Haake (1982), 7 Barbieri and Panieri (2004), 8 Van Hinsbergen et al. (2005), 9 Violanti et al. (2011), 10 Corbí (2010), 11 Van Morkhoven et al. (1986), 12 De Stigter et al. (1998), 13 Baggley (2000), 14 Gebhardt (1993), 15 Berggren and Haq (1976), 16 Pérez-Asensio et al. (2012), 17 Poag and Tresslar (1981), 18 De Stigter et al. (1998), 19 Bandy and Chierici (1966), 20 De Rijk et al. (2000), 21 De Rijk et al. (1999); 22 Sen Gupta and Machain-Castillo (1993), 23 Murray (2006), 24 Bizon and Bizon (1984), 25 Mendes et al. (2012), 26 Ohga and Kitazato (1997), 27 Milker and Schmiedl (2012), 28 Alve (2003), 29 Austin and Evans (2000), 30 Schmiedl et al. (1997), 31 Suokhrie et al. (2021), 32 Russo et al. (2007) and 33 (Hayward, 2004).

Species	min depth	max depth	SD
Amphicoryna spp.*	9	2860	1425.5
*Anomalinoides helicinus**	600	2000	700
Asterigerina planorbis	200	400	1000
Bolivina dilatata	15	3000	1492.5
Bolivina spathulata	30	3547	1758.5
*Bulimina aculeata**	5	4000	1997.5
Bulimina elongata	16	200	92
Bulimina mexicana	100	2000	950
*Bulimina striata**	100	800	350
*Cancris oblongus**	30	500	60
Chilostomella spp.*	700	1900	600
*Cibicidoides bradyi**	200	3000	1400
*Cibicidoides pseudoungerianus/ungerianus**	50	4000	1975
*Cibicidoides kullenbergi**	1000	4000	500
Cibicides lobatulus	20	1300	640
*Cibicidoides pachyderma**	30	4000	1985
*Cibicides dutemplei**	100	600	250
Dentalina spp.*	30	1200	585
Fursenkoina acuta	0	600	300
Globobulimina spp.*	1000	1500	250
Globobulimina turgida	30	150	60
*Globocassidulina subglobosa**	50	4000	1975
*Gyroidina altiformis**	30	600	285
*Gyroidina soldanii**	100	5000	2450
*Karreriella bradyi**	100	3000	1450
Lenticulina spp.*	600	1500	450
*Martinotiella communis**	200	3000	1400
*Melonis barleeanus**	13	3974	1980.5
*Melonis pompilioides**	100	3000	1450
*Melonis soldanii**	90	1000	455
Nodosaria spp.*	30	1700	235
Nonion fabum	0	200	100
Oridorsalis stellatus	250	1500	625
*Oridorsalis umbonatus**	65	4000	1967.5
*Planulina ariminensis**	70	1300	615
Pullenia bulloides	60	4000	1970
*Pullenia quinqueloba**	50	2000	975
*Sigmoilopsis schlumbergeri**	57	1500	721.5
*Sphaeroidina bulloides**	100	2000	950
Stainforthia fusiformis	0	2200	1080
Textularia calva	0	2000	1000
Trifarina bradyi	0	600	300
*Uvigerina peregrina**	100	4400	2150
*Uvigerina rutila**	200	1000	1400

Therefore, to obtain an independent quantification of the palaeobathymetry we estimated the palaeo-water depth using one of several more recently developed equations (e.g. Hohenegger, 2005; Hohenegger et al., 2008; Avnaim-Katav et al., 2016; Milker et al., 2017) based exclusively on the benthic foraminiferal fauna. In this study we apply the transfer function of Hohenegger (2005), since this is considered reliable in deeper environments and has been evaluated by Baldi and Hohenegger (2008) in the Vienna Basin and by Pérez-Asensio et al. (2012) in the Guadalquivir basin. The equation, here used as modified by Hohenegger et al. (2008) and Baldi and Hohenegger (2008) includes the relative abundances of each species and their depth ranges (Table 1):

Table 2
Microhabitat preferences of benthic foraminifera from the Rio Mendelin section and ODP Site 976: epifauna (0–0.7 cm BSWI), infauna (>0.7 cm BSWI) and deep infauna (> 3 cm BSWI).

Oxic	Suboxic (Groups A and B)	Dysoxic
Cibicidoides brady	*Amphicoryna* spp.	*Bolivina dilatata*
Cibicides dutemplei	*Anomalinoides helicinus*	*Bolivina reticulata*
Cibicidoides kullenbergi	*Asterigerina planorbis*	*Bolivina seminuda*
Cibicides lobatulus	*Bulimina elongata*	*Bolivina spathulata*
Cibicidoides pachyderma	*Bulimina striata*	*Chilostomella* spp.
Cibicidoides pseudoungerianus	*Cancris oblongus*	*Fursenkoina acuta*
Cibicidoides ungerianus	*Dentalina* spp.	*Globobulimina* spp.
Sphaeroidina bulloides	*Epistominella trinacria*	*Globobulimina turgida*
	Globocassidulina subglobosa	*Stainforthia fusiformis*
	Gyroidina altiformis	
	Gyroidina soldanii	
	Karreriella bradyi	
	Lenticulina spp.	
	Martinotiella communis	
	Melonis barleeanus	
	Melonis pompilioides	
	Melonis soldanii	
	Nodosaria spp.	
	Nonion fabum	
	Oridorsalis stellatus	
	Oridorsalis umbonatus	
	Planulina ariminensis	
	Pullenia bulloides	
	Pullenia quinqueloba	
	Sigmoilopsis schlumbergeri	
	Textularia calva	
	Trifarina bradyi	
	Uvigerina peregrina	
	Uvigerina rutila	

$$Paleodepth\ (m) = \sum_{j=1}^{k}\left[\left(l_j{*}n_j\right)/d_j\right] \Big/ \sum_{j=1}^{k}\left(n_j/d_j\right)$$

where n_j is the relative abundance of the n^{th} species, l_j the mean species depth, and d_j the dispersion. As suggested by Hohenegger (2005), to calculate the mean species depth for shallower marginal basins (e.g., Rio Mendelin section) we used the geometric means, while for deeper basins (ODP Site 976), we used the arithmetic mean in order to avoid underestimation. The foraminifera used in the calculation are all autochthonous species and reported in Table 1.

3.4. Estimation of bottom-water oxygen levels

The benthic foraminiferal distribution within the sediment depends on the organic flux and oxygenation at the sea floor (Jorissen et al., 1995; Van der Zwaan et al., 1999). Consequently the microhabitat is used as an indicator of dissolved oxygen (Kaiho, 1994), since species with deep infaunal (>3 cm below the sediment-water interface; BSWI) and intermediate infaunal (>0.7 cm BSWI) microhabitats thrive when oxygen levels are reduced, while epifaunal ones (0–0.7 cm BSWI) prefer better oxygenated bottom waters (e.g. Corliss and Chen, 1988; Jorissen et al., 1995; Schmiedl et al., 2000; Gooday, 2003).

These microhabitat preferences, reflected by morphological characteristics (size, wall thickness, shape: e.g., Corliss and Chen, 1988) can be used to define three groups of benthic foraminifera (Table 2) indicating respectively oxic (>1.5 ml/l O_2), suboxic (0.3–1.5 ml/l O_2) and dysoxic (0.1–0.3 ml/l O_2) environments (Kaiho, 1991; Kaiho, 1994; Kaiho, 1999). In addition, within the dysoxic indicators three different groups (A, B, C) have been defined (Kaiho, 1994) where group C includes species that have intermediate characteristics between suboxic and dysoxic markers. Using these indicators, the Benthic Foraminiferal Oxygen Index is calculated (BFOI; Kaiho, 1991; Kaiho, 1994; Kaiho, 1999) obtaining five different conditions of dissolved oxygen: anoxic (−55), dysoxic (−50 to −40), suboxic (−40–0), low oxic (0–50), and high oxic

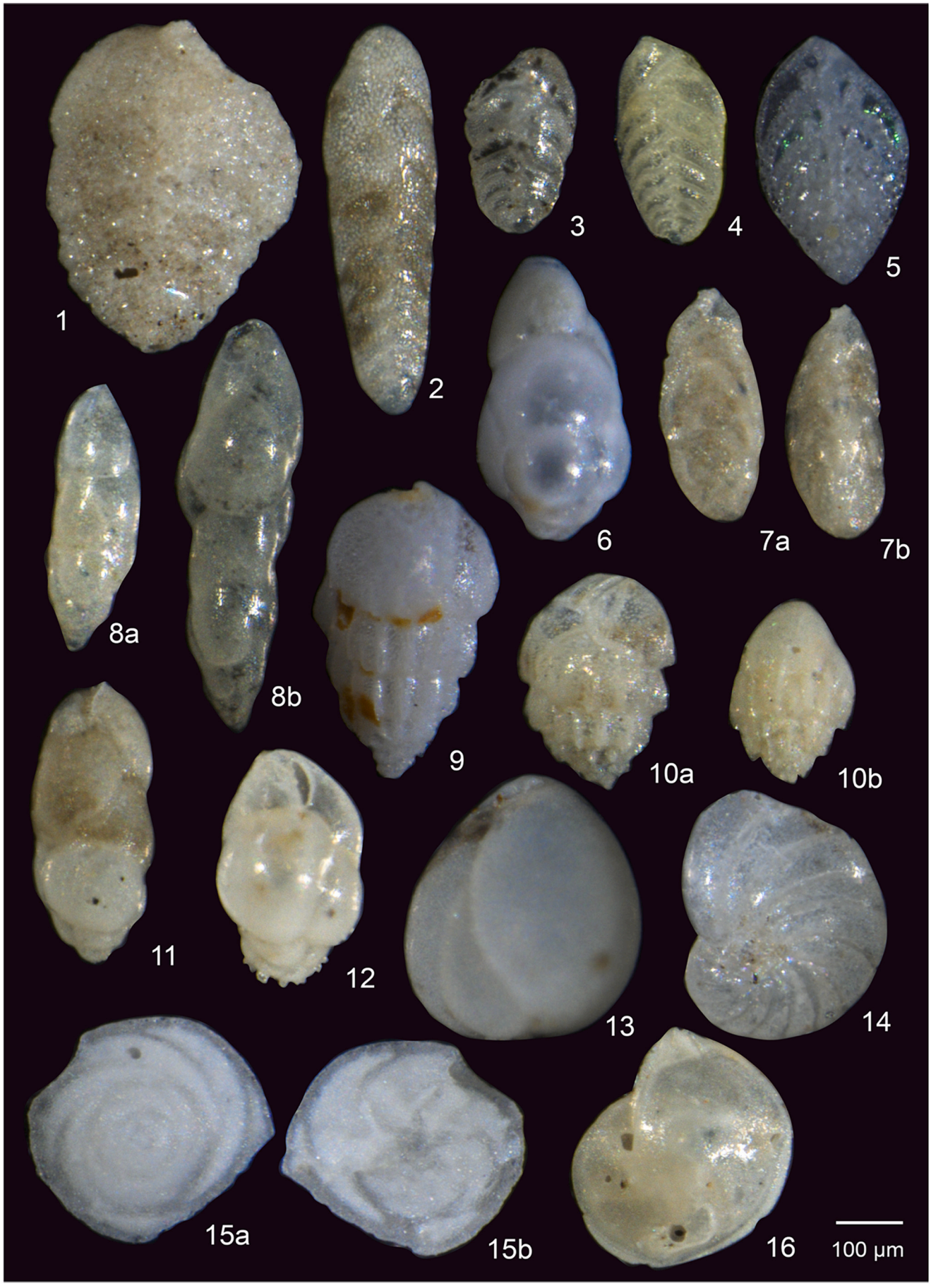

(caption on next page)

Plate 1. Optical microscope photos of the most abundant (>3%) benthic foraminifer species of Rio Mendelin section. **1** *Textularia calva*; **2** *Bolivina seminuda*; **3** *Bolivina spathulata;* **4** *Bolivina dilatata*; **5** *Bolivina reticulata*; **6** *Stainforthia fusiformis;* **7 a, b** *Trifarina bradyi;* **8 a, b** *Fursenkoina acuta*; **9** *Bulimina striata* var. *mexicana*; **10 a, b** *Bulimina striata*; **11** *Bulimina elongata*; **12** *Bulimina aculeata*; **6**; **13** *Globobulimina turgida*; **14** *Nonion fabum*; **15 a, b** *Asterigerina planorbis*: **a** spiral view, **b** umbilical view; **16** *Lenticulina* sp. Scale bar = 100 μm.

(50–100). The BFOI proved to accurately reproduce long-term dissolved oxygen changes in the Marmara Sea (similar bottom-water conditions as in the Mediterranean) and therefore it can probably be used to evaluate oxygen levels in the Mediterranean too (Kaminski, 2012).The interpretation of the BFOI is prone to bias when very low-diversity assemblages are studied and consequently, this estimate has not been applied to samples with a Shannon index ≤1 (Kaiho, 1994). Moreover, studies on recent benthic foraminifera suggest that quantitative reconstruction of oxygen levels higher than 1 ml/l is probably not feasible (Murray, 2001; Jorissen et al., 2007 and references therein).

The BFOI has been calculated following the formula (Kaiho, 1994):

$$\mathrm{BFOI} = \left(\frac{O}{(O+D)}\right)*100$$

where O and D (with O > 0) are the numbers of oxic and dysoxic indicator species, respectively.

When O = 0 and $I > 0$, the equation:

$$\mathrm{BFOI} = \left(\left(\frac{I}{(I+D)}\right) - 1\right)*100$$

is used instead, where I is the sum of suboxic indicators. The suboxic indicators in group C are excluded from the formula (Kaiho, 1994) although the species are used for the paleoenvironmental interpretations.

It is important to mention that oxygen estimates based on any indices can be subject to problems related to, for example, existence of an ecosystem oxygen gradient, coexistence of species with different microhabitat preferences, time-averaged samples or the interplay between export productivity and oxygenation in defining the preferred microhabitat (Jorissen et al., 2007).

3.5. Stable isotope measurements

Epifaunal taxa such as *Cibicides* spp. and *Cibicidoides* spp. were observed to secrete calcite close to equilibrium with the ambient sea water, displaying minor vital and minimal ontogenetic effects (Theodor et al., 2016a; Theodor et al., 2016b; Jöhnck et al., 2021 and references therein), and therefore 2 to 10 specimens (based on the availability) of *Cibicidoides pachyderma* were picked from ODP Site 976 (core 61) samples for stable isotope analyses. The actual contact between Miocene and Pliocene sediments was not recovered at this site. Nonetheless, our new stable isotope data from three samples of 62×-CC section confirms their Messinian age (see Section 5.4) and consequently attribute, paired with stratigraphic markers (Bulian et al., 2021), an early Pliocene age for core 61. The analysis was only possible until 571.18 m because specimens from the younger part of the sequence were affected by secondary calcite precipitation on the surface and within the aperture, which persisted even after ultrasonic cleaning. For the Rio Mendelin section, other species were chosen given the absence of *C. pachyderma*. *Epistominella trinacria* was picked in the basal two samples because the assemblage in the lowermost level is monospecific and in the next level nearly so (88.6%). In the next samples *Cibicides dutemplei* was picked, while starting from 1 m and going upwards, *Cibicidoides ungerianus* was chosen. More than one species was picked where possible, to obtain intraspecific correction factors. All measurements were transformed to *C. ungerianus*. This species has been reported to yield comparable values as *C. pachyderma* (Kaboth et al., 2017). Based on two paired measurements the *E. trinacria* values were corrected by adopting a value equal to the average offset from the *C. dutemplei* values (−0.21 for $\delta^{13}C$ and 1.46 for $\delta^{18}O$ values). The *C. dutemplei* record and the corrected *E. trinacria* data points were then all adjusted using the average offset established from six paired measurements between *C. dutemplei* and *C. ungerianus* (0.33 for $\delta^{13}C$ and −0.03 for $\delta^{18}O$ values). Samples from the Barranco del Negro section were not picked for stable isotope analyses because part of the foraminifera are not in situ.

The stable oxygen and carbon isotope analyses were performed with a Finnigan MAT 253 mass spectrometer connected to a Kiel IV carbonate preparation device at the Christian-Albrecht University in Kiel (Germany). Sample reaction was induced by individual acid addition (99% H_3PO_4 at 75 °C) under vacuum. The evolved carbon dioxide was analysed eight times for each individual sample. As documented by the performance of international [NBS19: +1.95 ‰ VPDB (^{13}C), −2.20 ‰ VPDB (^{18}O); IAEA-603: +2.46 ‰ VPDB (^{13}C), −2.37 ‰ VPDB (^{18}O)] and laboratory-internal carbonate standards [Hela1: +0.91 ‰ VPDB (^{13}C), +2.48 ‰ VPDB (^{18}O); HB1: -12.10 ‰ VPDB (^{13}C), −18.10 ‰ VPDB (^{18}O); SHK: +1.74 ‰ VPDB (^{13}C), −4.85 ‰ VPDB (^{18}O)], analytical precision of stable isotope analysis is better than ±0.08 ‰ for $\delta^{18}O$ and better than ±0.05 ‰ for $\delta^{13}C$. The obtained values were calibrated relative to Vienna Pee Dee Belemnite (VPDB).

4. Results

4.1. Malaga Basin: Rio Mendelin section

4.1.1. Micropalaeontology and stable isotopes

The lowermost 2 m of the Rio Mendelin section (Lago-Mare deposits) are barren of foraminifera and contain high abundances of ostracods, mainly *Cyprideis* sp. (Fig. 8). At the base of the Pliocene benthic foraminifera appear and remain present throughout the section. Considering the distribution and the good preservation of the specimens, which do not show any signs of transport or alteration, the foraminifera can be considered in situ. Optical microscope pictures of the species are shown in Plates 1 and 2.

The first benthic foraminiferal species appearing in the Zanclean is *Epistominella trinacria* which characterises the lowermost 60 cm of the section (2.1–2.7 m) (Figs. 8, 9). This species disappears almost completely at the base of the grey layer when other species appear: *Fursenkoina acuta*, *Globobulimina turgida*, and *Stainforthia fusiformis* (Fig. 8) which are limited to this grey interval. At the same level, several other species appear which remain present throughout the record (Fig. 9). The most abundant at this level is *Nonion fabum* (~ 50%).

Cluster analysis resulted in two main Clusters 1 and 2 (Fig. 10A and B, top panel). Cluster 2 is composed of two subclusters, Clusters 2.1 and 2.2, the first composed of a total of four subclusters (Fig. 10). These clusters group benthic foraminiferal species based on their distribution, enabling the distinction of three stratigraphic units (Units 1 to 3; Fig. 9). Cluster 1, defining Unit 1, dominates from 2 to 2.5 m in the section and is represented by only one species, *E. trinacria*. The following 0.5 m (2.5–3 m, in the grey layer), Unit 2, is dominated by *F. acuta*, *G. turgida*, *B. dilatata* and *S. fusiformis* forming Cluster 2.2. Overlapping with Cluster 2.2 but continuing until ~4 m, is Cluster 2.1.2 A. Highest abundances are reached by *N. fabum* (~50%), *B. striata* (~25%) and *Lenticulina* spp. (up to ~20%). The other species of Cluster 2.1.2 A show relative abundances ranging between ~5 and 12% (Figs. 9 and 10). At ~4 m, Cluster 2.1.2 B becomes dominant (Fig. 10B). *Cibicides dutemplei*, *C. pseudoungerianus* and *C. ungerianus* dominate the assemblage reaching abundances of ~15–16% (Figs. 9 and 10). Apart from *Textularia calva* (~10%), the remaining species are subordinate, and most do not reach 5% of abundance (Figs. 9 and 10). Cluster, 2.1.2C is composed of

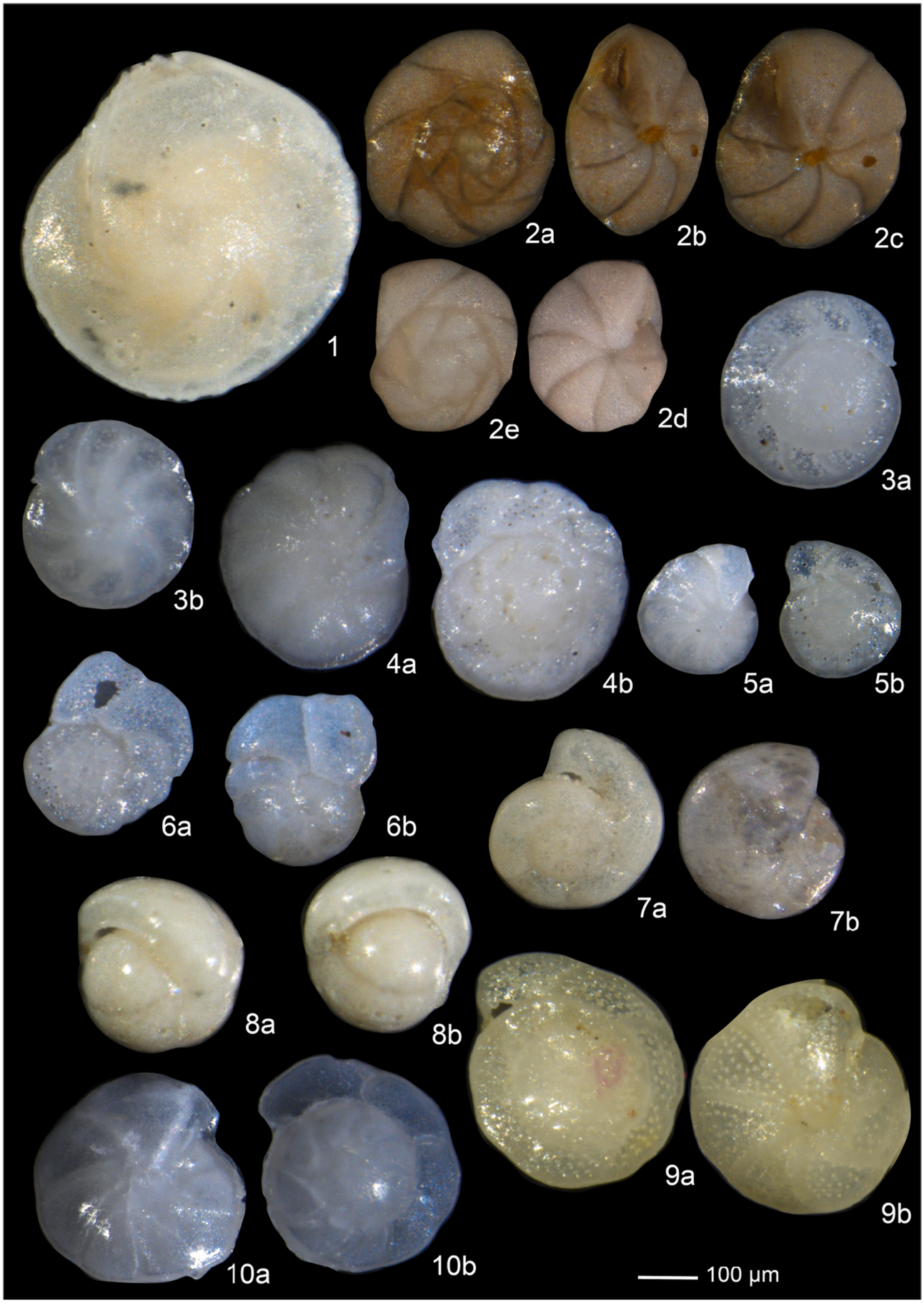

(caption on next page)

Plate 2. Optical microscope photos of the most abundant (>3%) benthic foraminifer species of Rio Mendelin section. **1** *Lenticulina* sp.; **2** *Epistominella trinacria*: **a, e** spiral view, **b** apertural view, **c, d** umbilical view; **3** *Cibicidoides pachyderma*: **a** spiral view, **b** umbilical view; **4** *Cibicidoides ungerianus*: **a** spiral view, **b** umbilical view; **5** Cibicidoides pseudoungerianus: **a** spiral view, **b** umbilical view; **6** *Cibicides lobatulus*: **a** spiral view, **b** umbilical view; **7** Gyroidina soldanii: **a** spiral view, **b** umbilical view; **8** *Pullenia bulloides*: **a** lateral view, **b** apertural view; **9** Cibicides dutemplei: **a** spiral view, **b** umbilical view;**10** Oridorsalis stellatus: **a** spiral view, **b** umbilical view. Scale bar = 100 μm.

Pullenia bulloides and *Trifarina bradyi*, both showing an upward increasing trend (Fig. 9) and reaching their maximum abundance around the top of the section (~16 and 5% respectively). These taxa display a trend in phase with Cluster 2.1.2 A and Cluster 2.2 (Figs. 9 and 10). Unit 3 (3–23.5 m), is characterised by a regular interchange (every 3–4 m until the top of the section) of the most abundant Clusters 2.1.2 A (+Cluster 2.1.2C and Cluster 2.2) and 2.1.2 B, marking a juxtaposition between the two assemblages which appears to be cyclical.

The benthic foraminiferal diversity rises throughout the record (H index from 0 to ≥ ~2.9; Fig. 10 B). The %P increases from 0% to ~40% at the base of the section to remain stable at ~40–50%. A change in the benthic foraminiferal microhabitat preferences shows as an interchange between prevailing infaunal or epifaunal taxa (Fig. 10), mimicking the juxtaposition between Clusters 2.1.2 A (+Clusters 2.1.2C and 2.2) and Cluster 2.1.2 B. Deep infauna is present only in the grey layer of Unit 2 with a maximum of ~20%. Since the three low-diversity samples at the base were excluded from the oxygen estimate, the BFOI is lowest in the grey layer (~3–12; Fig. 10 B), and above 4 m increases and oscillates between 60 and 90, showing the highest values (~85–90) in correspondence with intervals where epifaunal species dominate (Fig. 10 B).

From 3 m upward, planktic foraminifera (Supp. 1) become increasingly abundant and the assemblage is dominated by *Globigerinoides* spp., *Globoturborotalita apertura* and *Globigerina bulloides*. Less abundant species include *Globigerinita glutinata*, *Orbulina universa* and *Neogloboquadrina acostaensis*. At 7.4 m a few *Globorotalia margaritae* are identified.

The benthic stable oxygen and carbon isotopes of the Rio Mendelin section are shown in Fig. 10 B (panels to the right). After the lowermost two samples with values of ~−2 ‰, the benthic $\delta^{13}C$ remains stable at ~ − 1 ‰ with only two oscillations towards lighter values at 7 and 23.5 m. The benthic $\delta^{18}O$ trend is very similar. The lowermost samples show an increasing upward trend from ± − 0.7 ‰ to ±0.6 ‰ at 3 m in the section and then remains stable throughout the record except two negative excursions at the same stratigraphic position as in the $\delta^{13}C$ curve.

4.1.2. Palaeo-water depth reconstruction

Since the benthic foraminifera are considered indigenous, palaeodepth has been calculated for the Rio Mendelin section (Fig. 11). A first approximation of the palaeodepth was derived from the $\%P = 100*P/(P + B)$ (Van der Zwaan et al., 1990; Fig. 10 B). Applying the regression function (Van der Zwaan, *op. cit.*, eq. 7), the palaeodepth varies from a minimum of <50 m at the base of the section ($\%P$ = 0–10%) to a maximum depth of ~150 m ($\%P$ = 40%) at 10 m. The mean palaeodepth oscillates around 100 m. The palaeodepth reconstruction based on the transfer function of (Hohenegger, 2005; Hohenegger et al., 2008) corresponds with the %P until 7 m in the section. From here upwards, the difference between the reconstructions amounts to some 50–80 m.

4.2. Nijar Basin: Barranco del Negro section

Benthic and planktic foraminifera are present in the entire Barranco del Negro section. Many planktic specimens are overgrown by secondary calcite, but the benthic specimens are generally well preserved (Plates 3 and 4). Although scarce, up to 2 m in the section disarticulated ostracods have been identified, mainly the brackish *Cyprideis* sp. Brackish gastropoda are present until the calcarenite (0.5 m in Fig. 12; Plate 3). A bivalve-rich horizon is identified at 0.64 m, and bivalve shells are also present at 2 and 2.3 m in the section without being concentrated in a horizon (Fig. 6 C). At the top of the section (3.5 m), burrows are observed, probably of the genus *Thalassinoides*.

The most abundant benthic foraminiferal species in the Barranco del Negro record (Fig. 12) are *Cibicides lobatulus*, *Bolivina spathulata* and *Elphidium* spp., with subordinate *C. ungerianus*, *Cibicidoides kullenbergi* and *Planulina ariminensis* (~10%). The lowermost 0.5 m of the section are dominated by *B. dilatata, Elphidium* spp. (~15%), *Rectouvigerina cylindrica, P. ariminensis, Uvigerina rutila* and *C. lobatulus* (all ~10%). Above the black and grey layer at 0.5 m, *Chilostomella* spp. (~15%), *Ammonia* spp. (~10%), and *Globobulimina* spp. (~5%) sharply increase but remain present only for 1 m in the section (0.5–1.5 m). The interval between 1 and 2 m is characterised by relatively high abundances of *E. trinacria* (~15–25%) and *B. spathulata* (~15%). From 2 m until the top of the section *Spiroplectinella deperdita* (~ 15–20%), *Cibicides refulgens* (~10%), *P. bulloides* (~5–10%), *Lenticulina* spp. (~8%), and *Sphaeroidina bulloides* (~7%) show their highest abundances.

The Shannon diversity index of the Barranco del Negro section shows a relatively stable trend throughout the record with an average value of 2.6. The %P shows an upward decreasing trend with the highest average values at the base of the section (~95%) and lower values at the top (~75%; Fig. 12).

The dominant planktic foraminiferal species present in the Barranco del Negro record are *G. bulloides*, *Globigerinoides* spp. and sinistrally coiled (sx) *N. acostaensis*, with subordinate *O. universa* and *Globorotalia miotumida*. The uppermost two samples contain some specimens of *G. margaritae*. The presence in almost every sample of typical Messinian species like *G. miotumida* and *N. acostaensis* sx (Table 3; Sierro et al., 1993) suggests that reworking has affected the samples. Reworking is further suggested by the presence of brackish ostracod and gastropod species, occurring together with marine fauna at the base of the section. The concomitant presence of lower neritic to bathyal benthic foraminiferal species and shallow-water taxa (see Section 5.2.1) indicates that reworking also involved benthic species.

4.3. Sorbas basin: Zorreras section

In the Zorreras section foraminifera are very scarce but well preserved, even though their surface is sometimes covered by minerals. Benthic foraminifera appear at the base of the grey layer, which is rich in calcareous nodules. From that level upward very scarce specimens of *N. fabum* and even fewer *Elphidium* spp. and *C. lobatulus* are present in the analysed samples, until the top of the section, right on top of the transgressive bivalve lag (Fig. 5 B). Planktic foraminifera are absent.

4.4. Alboran Basin: ODP Site 976

4.4.1. Micropalaeontological content and stable isotopes

In the lower Pliocene sediments of ODP Site 976 benthic and planktic foraminifera show well preserved tests, even though some are overgrown with secondary calcite. Apart from shallow-water benthic foraminiferal species (*Elphidium* spp., *Rosalina* spp., discorbids and *Cibicides lobatulus*; see 3.1) we consider the foraminifera in situ and suitable for palaeoenvironmental analyses. Ostracods were absent at this site. Optical microscope photos of the benthic foraminiferal species are shown in Plates 5 and 6.

Benthic foraminiferal distributions are shown in Fig. 13. The base of the studied core is characterised by peak abundance of *Bulimina aculeata* (35%), which nearly disappears at 573 m below sea floor (mbsf), and by *Melonis barleeanus* (~25%), *Lenticulina* spp. (~18%), *S. bulloides*,

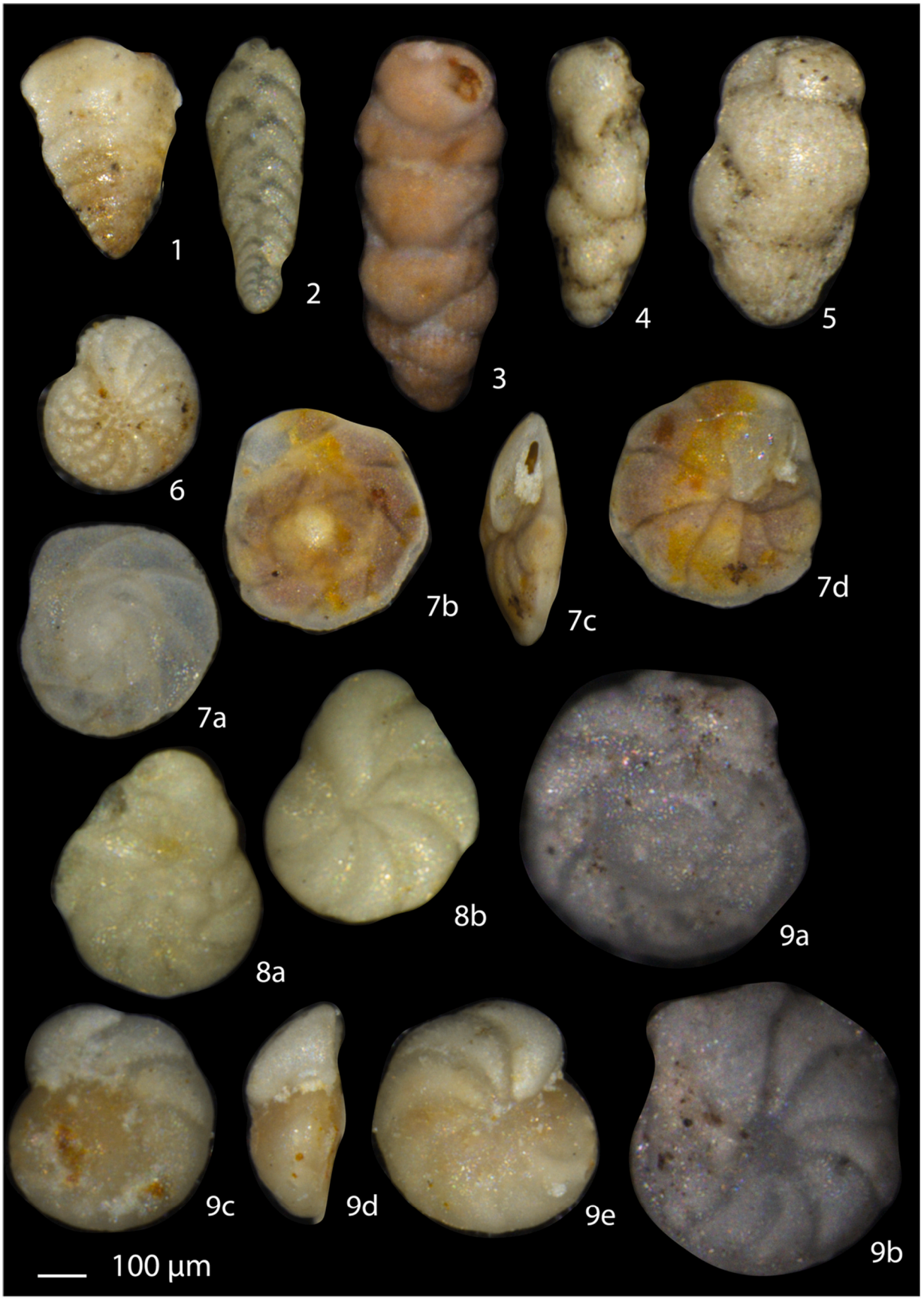

Plate 3. Optical microscope photos of the most abundant (>3%) benthic foraminifer species of Barranco del Negro section. **1** *Spiroplectinella deperdita*; **2** *Bolivina spathulata*; **3, 4** *Rectouvigerina cylindrica*; **5** *Uvigerina rutila*; **6** *Elphidium* sp.; **7**. *Epistominella trinacria*: **a, b** spiral view, **c** apertural view, **d** umbilical view; **8** *Valvulineria* sp.: **a** spiral view, **b** umbilical view; **9** *Cibicides ungerianus*: **a, c** spiral view, **d** apertural view, **b, e** umbilical view. Scale bar = 100 µm.

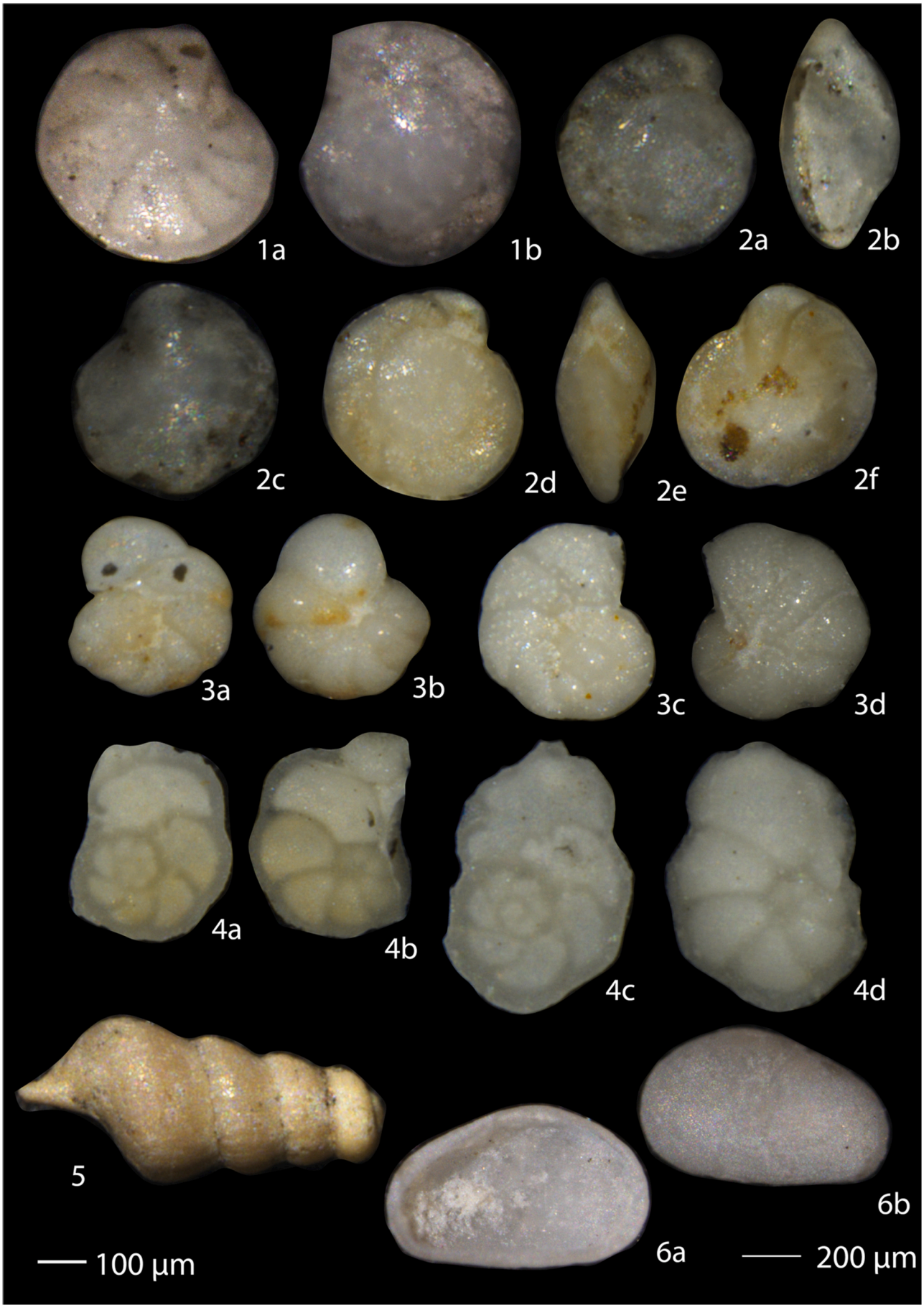

(caption on next page)

Plate 4. Optical microscope photos of the most abundant (>3%) benthic foraminifer species and one gastropod and ostracod species of Barranco del Negro section. **1** *Cibicidoides pseudoungerianus*: **a** spiral view, **b** umbilical view; **2** *Cibicidoides kullenbergi*: **a, d** spiral view, **b, e** apertural view, **c, f** umbilical view; **3** *Cibicides lobatulus*: **a, c** spiral view, **b, d** umbilical view; **4** *Cibicides refulgens*: **a, c** spiral view, **b, d** umbilical view; **5** gastropod; **6** *Cyprideis* sp. Scale bar = 100 μm, 200 μm for the ostracod.

Table 3
Stratigraphic position of selected samples from the Barranco del Negro section where the bivalve shells/g, ostracods/g, percentages of Messinian species like *G. miotumida* and *N. acostaensis* sx were counted.

Position	Shells/g	Ostracods/g	% *G. miotumida*	% *N. acostaensis* sx
3.84	3.29	3.29	0.71	1.22
2.94	0.00	0.00	1.45	4.17
2.04	14.74	6.98	0.48	0.72
1.44	1.25	1.25	0.42	0.72
1.04	1.18	1.42	0.92	8.76
0.69	49.81	3.94	0.00	2.33
0.54	23.39	3.37	0.00	1.48
0.35	21.60	0.22	1.03	4.94
0.2	2.70	0.19	0.51	5.58

Nodosaria spp. and *M. soldanii* (10–12%) which remain present throughout the record. From 572.4 mbsf, the abundances of *Globocassidulina subglobosa* (~20–40%), *Uvigerina peregrina* (~30%), and *B. striata* (~12%) increase. At 569 mbsf, coinciding with a sharp decrease of *U. peregrina*, the percentage of displaced shallow-water species rises to ~10% (Fig. 13).

The dendrogram divides the benthic assemblages in two main Clusters 1 and 2 and three subclusters (Clusters 2.1, 2.2.1 and 2.2.2), allowing the identification of Units 1 to 4 (Fig. 14) characterised by specific benthic foraminiferal assemblages. The two species of Cluster 1 dominate the lowermost 0.5 m of the studied interval and represent Unit 1 (573.5–573.1 mbsf). *Bulimina aculeata* (35%) and *C. dutemplei* (4%) are also present in the overlying Unit 2, before disappearing almost completely in Unit 3. Less abundant in Unit 1 are the species forming Cluster 2.2.2 which dominate Unit 2 (Fig. 14B). Cluster 2.2.2 shows maximum abundance between 573.1 and 572.5 mbsf (Fig. 14A). Most abundant within Cluster 2.2.2 are *M. barleeanus* (30%) and *Lenticulina* spp. (20%) (Fig. 13). The other species in Unit 2 do not exceed 10% of abundance.

Unit 3 (572.5–569 mbsf) shows a change in benthic foraminiferal assemblages. The most abundant species of Unit 3 are comprised in Cluster 2.2.1 (Fig. 14A). Dominating Unit 3 are *G. subglobosa* (~40%), *U. peregrina* (~30%), *C. pachyderma* (~25%) and *C. ungerianus* (~20%). The other species of Cluster 2.2.1 vary between 6 and 12% (Fig. 13). In Unit 4 (569 mbsf until the top of the record) the assemblage of Cluster 2.1 joins Clusters 2.2.1 and 2.2.2 (Fig. 14B). Cluster 2.1 includes only two species, *Anomalinoides helicinus* (10%) and *Cancris oblongus* (3%; Fig. 13, 14A). Other relatively abundant species of Unit 4 are in Cluster 2.2.2 (Fig. 14B) including *Lenticulina* spp. (~16%), *Amphicoryna* spp. (~10%), *M. soldanii* (~10%) and *S. bulloides* (~8%) and in Cluster 2.2.1 including *G. subglobosa* (~15%) and *C. ungerianus* (~20%). Unit 4 also contains the higher percentages of displaced benthic foraminifera (~10%; Fig. 13).

The record is characterised by increasing diversity of benthic foraminifera (H index increasing upward; Fig. 14B).

Although the microhabitat preferences do not show major changes over the studied interval and infaunal species prevail with a stable 65%, the BFOI shows significant oscillations. Especially until 571.5 mbsf, the values vary from ~20 to a maximum of ~85. From this point onward they start a decreasing upward trend and change from 80 to 40 at the top of the record (Fig. 14B).

Planktic foraminifera represent ~95% of the foraminiferal assemblages (Fig. 14B). At 572.5 mbsf, the Pliocene markers *G. margaritae* and *Sphaeroidinellopsis* spp. appear, while the dominant planktic foraminifer species are *G. bulloides* (~50%), *G. apertura* (~40%) and *N. acostaensis* (~35%, Supp. 1. Less abundant species include *Globorotalia scitula*, *Globigerinoides* spp., *Neogloboquadrina atlantica*, *G. glutinata* and *O. universa*.

The benthic stable isotope record of Site 976 covers the 3 samples from core 62×-CC and the first ~3 m of the Pliocene sequence (Fig. 14B). The benthic $\delta^{13}C$ in the three Messinian samples show low values (−0.4 to 0 ‰). The $\delta^{18}O$ varies between 0.5 and 1.5 ‰. In the early Pliocene the values have shifted. The benthic $\delta^{13}C$ starts at 0.8 ‰ and the curve displays a continuously increasing upward trend to maximum values of ~1 ‰ at 571.3 mbsf. The Piocene benthic $\delta^{18}O$ record oscillates between ~−0.8 and 0–0.2 ‰ and shows a positive peak of ~0.6 ‰ at 572.8 mbsf.

4.4.2. Palaeo-water depth reconstruction

Because the benthic foraminifera are considered in situ, palaeodepth has been calculated for ODP Site 976. A first approximation of the palaeodepth can be derived from the $\%P = 100*P/(P + B)$ (%P; Van der Zwaan et al., 1990; Fig. 14B). Applying the regression function (Van der Zwaan et al., *op. cit.*, eq. 7), the palaeodepth was relatively stable and varied between a minimum of ~1000 m (%P = ~98%) and a maximum depth of ~1200 m. The palaeodepth reconstruction based on the transfer function (Fig. 15) of (Hohenegger, 2005; Hohenegger et al., 2008) yields lower values in 1/3 of the section, apart from the interval from 571 and 569 mbsf. The depth variability is also higher, and values vary between 950 and 1400 m. The difference between the reconstructions amounts to a maximum of 250 m in this interval, while throughout the rest of the record it varies between 0 and 200 m.

5. Discussion

5.1. Distinctive black/grey layers at the Miocene-Pliocene boundary

In the Barranco del Negro section (Nijar Basin), the MPB is marked by a distinct black layer (Fig. 2F) containing small gastropods, some ostracods from the genus *Cyprideis*, and abundant, probably reworked planktic foraminifera whereas the benthic foraminifera are mostly in situ. Elsewhere in the Nijar basin, for instance the Los Ranchos (Pérez-Asensio et al., 2021) and Barranco de los Castellanos sections (Aguirre and Sánchez-Almazo, 2004) the dark layer is absent, it may have been eroded when the high-energy shallow-water sands started depositing.

In the Rio Mendelin section (Malaga Basin), instead of a black layer a 75 cm thick grey clay layer was deposited at the base of the Zanclean, on top of 20 cm of yellowish silts. Also, in the Zorreras section (Sorbas Basin) a grey layer was found at the base of the Zanclean, containing carbonate nodules and overlying reddish continental late Messinian deposits (Fig. 2B). At the MPB in Eraclea Minoa the grey layer is overlying the Arenazzolo Formation (Fig. 2C; Brolsma, 1978; Pierre et al., 2006; Bulian, unpublished data). At deeper locations like ODP sites 975 (South Balearic Basin) and 974 (Tyrrhenian Basin; Iaccarino and Bossio, 1999; Iaccarino et al., 1999a; Fig. 2D, E), a grey layer is also observed at the MPB. The colour suggests organic matter accumulation and reduced oxygen levels, possibly caused by water column stratification, while the small clasts recorded in the Balearic Basin have been interpreted as the result of the first ingression of Atlantic waters into the Mediterranean Basin (Iaccarino and Bossio, 1999).

To better understand the depositional mechanisms of the dark layer and to assess whether water column stratification was present during the early Zanclean, it is important to consider the palaeoenvironment present in the Mediterranean before the reestablishment of an efficient Mediterranean – Atlantic connection (i.e., LM phase). As suggested by

(caption on next page)

Plate 5. Optical microscope photos of some of the most abundant (>3%) benthic foraminifer species identified at Site 976. **1** *Sigmoilopsis schlumbergeri*; **2** *Martinotiella communis*; **3** *Karreriella bradyi.*; **4a-b** *Lagena* spp.; **5** *Pseudonodosaria* sp.; **6** *Amphicoryna* sp.; **7** *Dentalina* sp.; **8** *Bulimina striata*; **9** *Bulimina aculeata* **10** *Uvigerina peregrina*; **11a-b** *Globobulimina* spp.; **12a-b** *Uvigerina rutila*; **13** *Globocassidulina subglobosa*; **14** *Sphaeroidina bulloides*; **15** *Anomalinoides helicinus;* **16** *Lenticulina* sp. Scale bar = 100 μm.

the presence of a Paratethyan brackish fauna (ostracods, molluscs and dinocysts) in upper Messinian sediments (e.g., Iaccarino et al., 1999b; Fortuin and Krijgsman, 2003; Orszag-Sperber, 2006; Rouchy and Caruso, 2006; Roveri et al., 2008; Guerra-Merchán et al., 2014; Stoica et al., 2016), the Mediterranean was most probably invaded by Paratethyan waters that created a brackish water layer (up to 250 m of thickness) on the Mediterranean surface (Marzocchi et al., 2016). Concordantly, lower surface water salinities have been estimated for the MPB from stable isotope data of Zakynthos Island (Kontakiotis et al., 2016). Considering the generally accepted deep basin MSC model (CIESM, 2008; Roveri et al., 2014a), the inflow of Paratethyan waters would lower the salinity of the Mediterranean marginal basins. At the MPB, with the increase of the Atlantic inflow, the marginal basins, filled with brackish water, would be invaded by more saline Atlantic waters which upon sinking created a stratified water column. This stratification could favour bottom water oxygen depletion and organic matter accumulation and explain the deposition of organic-rich layers. These black and grey layers thus represent the first reaction of the system to the reflooding, before mixing of the two water masses and establishment of normal marine conditions. For comparison, in the Black Sea region marine flooding events from the Mediterranean, characterised by the presence of foraminifera and calcareous nannofossils (Krijgsman et al., 2010; Radionova et al., 2012) create anoxic conditions as exemplified by a conspicuous dark layer barren of Paratethyan ostracods (Stoica et al., 2016). Such events have been identified in the late-Langhian (Sant et al., 2019), Pontian (Stoica et al., 2016) and even Pleistocene (Ross and Degens, 1974; Schrader, 1978) Black Sea sediments.

In the Mediterranean the organic-rich layer at the MPB assumes two different aspects, sometimes it materializes as a black layer and other times it displays only as a grey shade. Consequently, it appears that the conditions at the time of the Atlantic incursion in the Mediterranean were depending on the location and depth at the time of the reflooding. A strong water-mass stratification could lead to oxygen depleted environments and the accumulation of organic matter with the formation of a black layer. This could occur in basins located below the oxic/anoxic interface, while in basins located in the upper, more ventilated, part of the water column the bottom water properties were less affected. In the Sorbas Basin, where the latest Messinian environment was continental (Roveri et al., 2018 and this work), the grey layer materializes as a paleosol-like horizon and shows a gradual transition to a shallow marine environment.

The mechanism described for the deposition of the dark layers in the marginal basins is compatible with a LM scenario where the Paratethys water lid over the Mediterranean freshens the margins of the basin. However, such scenario for the deepest basins would mean a stratified water column and bottom water oxygen depletion already in the latest Messinian, comparable to sapropel deposition (e.g. Rohling et al., 2015 and references therein). From shallow and deep late Messinian Mediterranean sites any evidence of anoxia or reduced oxygen levels is missing and considering that the dark interval has been identified at the MPB of deep basins as well, the late Messinian palaeoenvironmental scenario must be revised. To explain a dark, organic-rich layer around the MPB all over the Mediterranean we suggest that the early Pliocene water column was stratified to some extent both in the marginal and the deeper basins. Such stratification could only form if Paratethyan brackish waters and/or fresh riverine inflow would have decreased the total salinity of the basin (not excluding a discrete vertical density gradient) allowing the Atlantic saltier waters to sink and develop a stratified water column.

At Site 976, the dark layer has not been observed but it might have been deposited and eroded, related to the vicinity to the Gibraltar gateway and the presence of a hiatus (see Section 2.2; Bulian et al., 2021).

5.2. Early Pliocene palaeodepth reconstructions

5.2.1. New data from this study: Marginal basins

5.2.1.1. Rio Mendelin section (Malaga Basin). According to the palaeodepth reconstruction based on Hohenegger (2005) and Van der Zwaan et al. (1990) and in agreement with the distribution of the benthic foraminifera, the lowermost metre of Pliocene sediments of the Rio Mendelin section in the Malaga Basin was deposited in an inner neritic environment (20–100 m) deepening to outer neritic depths (100–200 m) towards the top of the sampled record. The deepening-upward sequence is consistent with the transgressive nature of the earliest Pliocene sediments observed in the hinterland of the Alboran Basin, filling the previously excavated canyons, such as the Guadalhorce (e.g. Schoorl and Veldkamp, 2003). Analogous shallow marine environments have been recorded in several other southern Spanish marginal basins like Bajo Segura (shallow-water delta; Soria et al., 2005; García-García et al., 2011; Corbí and Soria, 2016), Sorbas (10–50 m; Roveri et al., 2018; this study), Vera (250 m; Fortuin et al., 1995; Caruso et al., 2020) and Nijar (250–350 m; Bassetti et al., 2006; Pérez-Asensio et al., 2021; this study).

5.2.1.2. Barranco del Negro section (Nijar Basin). The palaeodepth reconstruction of the Barranco del Negro section is primarily based on sedimentology, macrofauna (bivalves) and the ichnofossil *Thalassinoides*, since it cannot be à priori known which benthic foraminifera are reworked or displaced. Above the black-and-grey layer, the sediments are dominantly composed of bioclastic sandstones, lacking structure except some planar bedding. These sediments have been interpreted as deltaic (Aguirre, 1998) or shoreface deposits (Omodeo Salé et al., 2012; Donovan et al., 2021), overlying the black-and-grey layer in a ravinement (transgressive) surface. This limits the depositional depth to shelf, if lower shoreface probably not deeper than ~15–50 m. The precise depth is hard to define considering its dependence on the hydrographic setting (e.g. Anthony and Aagaard, 2020) *Thalassinoides* burrows and bivalve macrofauna including oysters usually occur in relatively shallow-water environments (Droser and Bottjer, 1987; Gingras et al., 2008; Roveri et al., 2018; Sharafi et al., 2021), although in more recent geological times they also occur at bathyal depths (Uchman and Demircan, 1999; Van Rooij et al., 2010). The shells in the bivalve bed at 0.64 m are mostly broken, indicating high-energy environments, but bivalves are better preserved higher in the section, and together with the *Thalassinoides* burrows at 3 m indicate somewhat quieter environments, suggesting that a slight deepening may have occurred. In the top of the section a few *G. margaritae* are present, indicating deposition of the section during (MPl1-) MPl2.

In the nearby Los Ranchos section Perez-Asensio et al. (2021) reconstruct a palaeodepth of 274 m (upper slope) immediately after the MPB. A black-to-grey layer is absent; Pliocene silts and sands are deposited on top of a marly interval attributed to the LM; reworking is only reported from these marls. The authors find shallowing upward after the lowermost 4 m of Pliocene sediments and consider benthic foraminifera indicating upper slope environments in these basal 4 m to be indigenous (e.g., *P. ariminensis*). Comparing the sections, the Pliocene silts and sands at Los Ranchos may have been deposited in a more distal environment than the inner-middle neritic calcarenites of the Barranco del Negro section reported here; however, if both sequences are

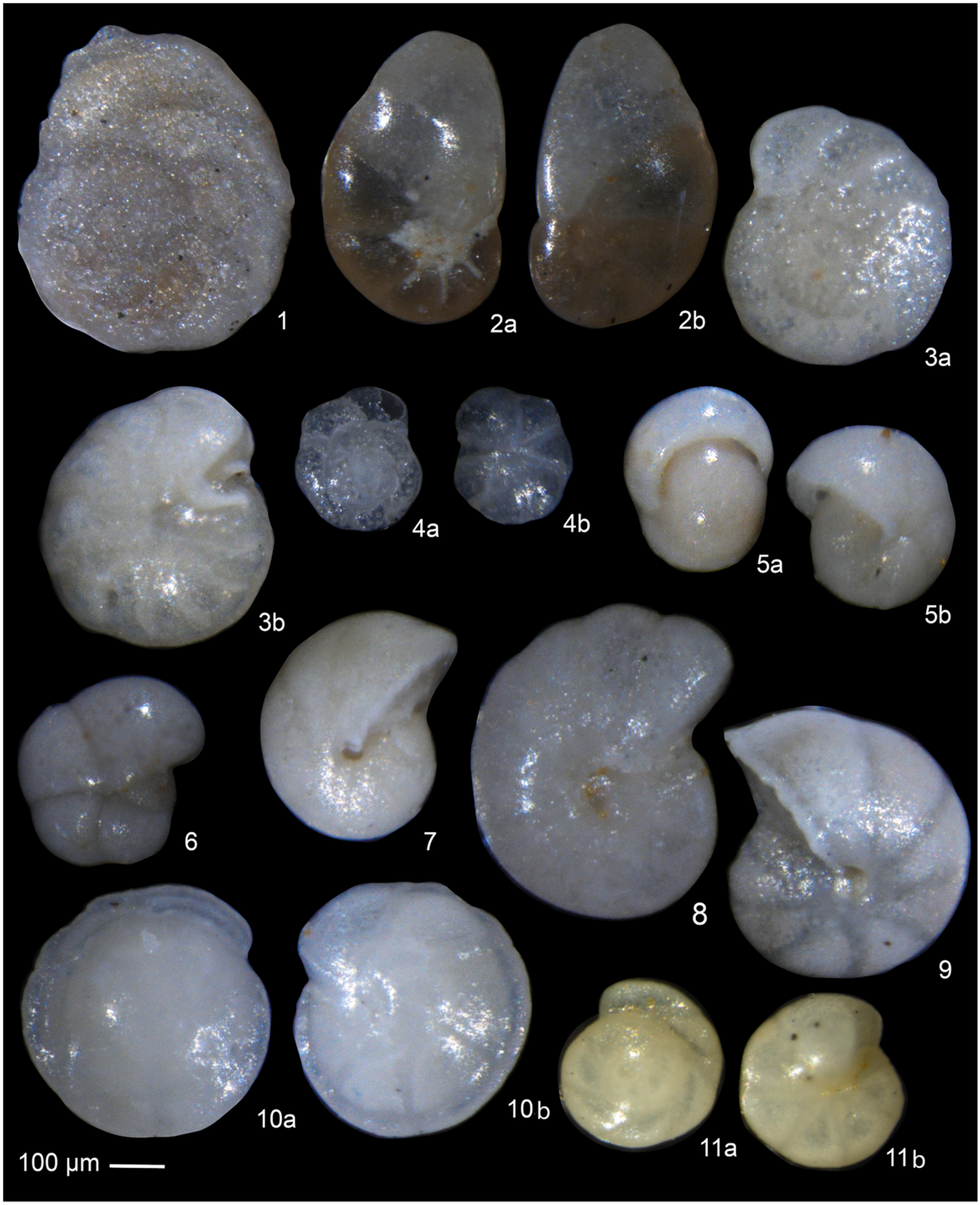

Plate 6. Optical microscope photos of some of the most abundant (>3%) benthic foraminifer species identified at Site 976. **1** *Planulina ariminensis*; **2** *Cancris oblongis:* **a** spiral view, **b** umbilical view; **3** *Cibicidoides ungerianus:* **a** spiral view, **b** umbilical view; **4** *Cibicidoides bradyi*: **a** spiral view, **b** umbilical view; **5** *Pullenia bulloides:* **a** apertural view, **b** lateral view; **6** *Pullenia quinqueloba;* **7** *Melonis soldanii*; **8** *Melonis barleeanus*; **9** *Melonis pompilioides;* **10** *Oridorsalis umbonatus*: **a** spiral view, **b** umbilical view; **11** *Gyroidina altiformis:* **a** spiral view, **b** umbilical view. Scale bar = 100 µm.

deposited immediately after the MPB we infer that at the Los Ranchos section no initial deepening after the MPB is recorded.

5.2.1.3. Zorreras section (Sorbas Basin). The Sorbas Basin was characterised by a continental environment during the latest Messinian stage (Roveri et al., 2018 and this work). The first Pliocene sediments deposited are grey sands rich in carbonate nodules and rare shallow-water benthic foraminifera, suggesting a very shallow, at times exposed environment similar to a paleosol. On top of this mostly emerged, continental facies, coastal sandy sediments were eventually deposited because of the rising sea level. The foraminiferal data are only qualitative; however, because of the absence of planktic foraminifera and the presence of shallow-water taxa like *N. fabum* and *Elphidium* spp. (Hayward et al., 2001; Murray, 2006; Milker, 2010; Tulbure et al., 2017) the Zanclean palaeodepth probably did not exceed 10–20 m.

In most marginal basins, Zanclean sediments are overlying continental and/or shallow, brackish LM facies (Fortuin et al., 2000; Guerra-Merchán et al., 2010; Caruso et al., 2020; Andreetto et al., 2021a and references therein; Andreetto et al., 2021b). In deeper marginal basins with age control based on planktic foraminifera, where the MPB is continuous and the MPl1 zone is complete, for instance at Eraclea Minoa (Brolsma, 1978; Sgarrella et al., 1997) and sections in Piemonte (Trenkwalder et al., 2008; Violanti et al., 2009) instantaneous refill to upper bathyal depth appears to have occurred immediately after the MSC. This implies a rapid deepening of at least 500 m at the base of the Zanclean. At Cava Serredi (Tuscany: Riforgiato et al., 2011) the refill seems to have been gradual; however, the actual base of the Zanclean may be missing since the MPB is reported to be continuous, but planktic foraminifera of MPl1 and MPl2 (*Sphaeroidinellopsis* spp., *G. margaritae*) are absent.

For shallower marginal basins, where age control is sub-optimal or absent, the picture is less clear and erosional surfaces are often reported to be associated with the MPB. Despite the erosional surface in the Cuevas del Almanzora section (Vera Basin), the MPl1 zone is reported to be complete. Caruso et al. (2020) reconstruct a water depth of >250 m immediately after the MPB, implying that the erosional surface has removed part of the LM deposits. This may be related to base level variations during the latest Messinian, as suggested by Gargani and Rigollet (2007), Stoica et al. (2016) and Andreetto et al. (2021b). At the Los Ranchos section (Nijar Basin) however, a palaeodepth of 274 m immediately after the MPB (Pérez-Asensio et al., 2021) is more likely caused by absence of the basal Pliocene since only *G. margaritae* and no *Sphaeroidinellopsis* spp. appear, and no benthic repopulation sequence is reported. In the Rio Mendelin section (Malaga Basin; this study) the contact between Messinian and Zanclean is gradual. A benthic repopulation sequence is present and few, but quite large *G. margaritae* occur above the grey layer.

5.2.2. Deep basin: ODP Site 976

The palaeo-water depth reconstructed for ODP Site 976 is bathyal (≥1000 m). A similar depth has been reported for the early Messinian at the same site (Bulian et al., 2022). Bathyal Zanclean palaeodepths have been reconstructed for the Eraclea Minoa and Capo Rossello sections in Sicily (Sgarrella et al., 1997; Barra et al., 1998: 600–800 m). In general, depth reconstructions for earliest Zanclean DSDP and ODP Sites have been in the order of upper- to mesobathyal (1000 m and more). DSDP Leg 42A, Site 371 (South Balearic Basin) was estimated to be 1200–1400 m deep (Wright, 1978). For Leg 107, Sites 652–654 (Tyrrhenian Basin) and Leg 161, Sites 974 (Tyrrhenian Sea) and 975 (Balearic Basin), the depth of MPl1 was also estimated to be bathyal (McKenzie et al., 1990; Sprovieri and Hasegawa, 1990; Iaccarino et al., 1999a). Based on planktic foraminifer biostratigraphy, the MPl1 in Site 975 (Iaccarino et al., 1999a) is complete. This would imply that the Pliocene refill of this – and other - deep basins happened instantaneously on a geological time sale, or alternatively, the basins were not dry at that time (e.g., Marzocchi et al., 2016; Stoica et al., 2016).

5.3. Benthic environments and repopulation

Lago-Mare deposits were either barren or containing brackish to fresh/continental faunas, including reworked fossils. Zanclean repopulation by benthic foraminifera shows similarities with repopulation following sapropel deposition. Jorissen (1999 and references therein) discerns general patterns when morphogroups are considered rather than individual species and defines morphogroups generally recognized in repopulation sequences: deep infauna tolerating extreme hypoxia in relatively stable environments (group A, e.g., *Chilostomella* and *Globobulimina* spp.); intermediate infauna, less tolerant to hypoxia (group B, elongated bi- and triserial taxa, e.g., bolivinids, buliminids, *Cassidulinoides* spp.); so-called 'phytodetritus species', small, biconvex and trochospiral taxa tolerating oxic to hypoxic, unstable environments and reproducing fast after seasonal input of fresh phytodetritus (group C, e.g., small *Epistominella*, *Eponides* and *Gyroidina* spp.). Depending on local environmental conditions, either group A or group C will precede group B in a repopulation event.

5.3.1. Marginal basins

5.3.1.1. Rio Mendelin section (Malaga Basin). In the Rio Mendelin section, the benthic foraminiferal assemblage immediately above the LM consists of monospecific *Epistominella trinacria* (Fig. 8; Plate 2). This species was described in Pliocene sapropels by Verhallen (1991) without further details; its occurrence is explained by analogy with other *Epistominella* species (mentioned in Group C cf. Jorissen, 1999). In recent environments *Epistominella* species have been associated with seasonal (spring/early summer episodes) deposition of fresh phytodetritus in oxic to sub-oxic (but not anoxic), otherwise oligotrophic environments (*E. exigua*: Gooday, 1988; Gooday, 1993; Smart et al., 1994; *E. vitrea*: Gooday and Hughes, 2002; Platon et al., 2005; Langezaal et al., 2006). In the fossil record *Epistominella* species were observed in Zanclean repopulation sequences (e.g., Sgarrella et al., 1997 (Sicily); Iaccarino et al., 1999b (Tyrrhenian Sea); Rouchy et al., 2001 (Cyprus); Aguirre et al., 2006 (Nijar Basin, Spain); Cipollari et al., 2013 (Adana Basin, Turkey); Kontakiotis et al., 2016 (Zakynthos, Greece); Caruso et al., 2020 (Vera Basin, Spain)) Their occurrence suggests that these environments were oxic to sub-oxic, oligotrophic but prone to seasonal variations in organic matter input.

The abundance of *E. trinacria* declines in the Rio Mendelin section after the lowermost, monospecific sample and the abundance of *Nonion fabum* increases to nearly 50% at the top of Unit 1 (Figs. 8, 9). *Nonion* spp. are versatile species, typical of high organic carbon content, phytodetritus and low oxygen conditions (Fontanier et al., 2002; Diz et al., 2004; Mendes et al., 2004; Mojtahid et al., 2006). Subordinate *Stainforthia fusiformis*, *Fursenkoina acuta* and *Globobulimina turgida* (Group A cf. Jorissen, 1999; Cluster 2.2) suggest a transition from a relatively oxic environment characterised by *E. trinacria* towards a more differentiated but more hypoxic environment towards Unit 2, the grey layer. At the same time, *Bulimina aculeata, B. elongata,* and *Bolivina dilatata* appear, taxa less tolerant to hypoxia (Group B cf. Jorissen, 1999). Towards the top of Unit 2, *B. seminuda* and *Oridorsalis stellatus* increase in abundance (cluster 2.1.2A, Fig. 10), suggesting continued repopulation in more oxic and less stable conditions towards the yellowish strata of Unit 3. This repopulation sequence is comparable to the one identified after Quaternary sapropels (S1, S5, S6) (Jorissen, 1999). Unit 3 reflects a normal marine assemblage under relatively stable, oxic conditions: the diversity (H) increases to 3, the BFOI, minimal in the grey layer supporting hypoxia, increases to 80% in Unit 3 (Fig. 10) and the hypoxia-tolerant species of cluster 2 decrease in abundance or disappear.

In the Rio Mendelin section, the Cluster 2.1.2 A assemblage prevails in the record until 4 m (Figs. 9 and 10), when Cluster 2.1.2 B

(*C. dutemplei*, *C. pseudoungerianus*, *C. ungerianus* and *Textularia calva*) becomes dominant. Although *Textularia* spp. are tolerant to food-enriched and oxygen-deficient conditions (Naeher et al., 2012), the more common *Cibicides/Cibicidoides*, epifaunal to shallow infaunal and with low tolerance to oxygen deficiency (Van der Zwaan, 1982; Jorissen et al., 2007), suggest relatively well-oxygenated waters and moderate productivity up to 6.4 m, in agreement with the BFOI, with values close to high-oxic environments (BFOI = ~90%; Fig. 10). Beginning in Unit 3, the benthic foraminiferal assemblages show a clear alternation between Cluster 2.1.2 A and Cluster 2.1.2 B (Fig. 10), hence between a mostly infaunal assemblage (buliminids, bolivinids, *N. fabum*, *Lenticulina* spp.) associated with high productivity and reduced oxygenation, and an epifaunal one, characterised by *Cibicides/Cibicidoides* species, indicating more oxic conditions. We suggest these cycles reflect an alternation of phases of lower versus higher nutrient input and riverine discharge associated with cyclical changes in the freshwater budget (see 5.4). The benthic and planktic $\delta^{18}O$ (Fig. 10 and Supp. 3) show heaviest values concomitant with Cluster 2.1.2 B peaks, suggesting astronomical control over the cyclicity.

In summary, in the Rio Mendelin section monospecific *E. trinacria* marks the start of benthic repopulation following the incursion of marine waters. The grey clays (Unit 2) more likely reflect water stratification related to further sea-level rise than influx of organic matter. Continued sea-level rise ameliorated circulation and ventilation, eventually supporting a diverse open marine benthic foraminiferal assemblage. Comparable repopulation sequences were described elsewhere in the Mediterranean (see above).

5.3.1.2. Barranco del Negro section (Nijar Basin). The calcarenites above the black and grey layer in the Barranco del Negro section suggest a nearshore, high-energy environment (see Section 5.3.1), but the reconstruction of palaeoenvironment and repopulation by benthic foraminifera is complicated by reworking (see 4.2; Table 3). The number of benthic foraminifera per gram of sediment (BF/g; Fig. 12), which is very low in the black and grey layer, rises steadily suggesting that the number of reworked foraminifera is relatively low, and more indigenous benthic foraminifera start occurring above the black-grey layer. In the first sample above the grey level *Chilostomella* and *Globobulimina* species appear which, if in situ, may be part of a repopulation sequence in an initially stable, hypoxic-anoxic environment (Group A of Jorissen, 1999).

The benthic foraminiferal species expected to thrive in a deltaic or shoreface palaeoenvironment is *C. lobatulus* (Hald and Korsun, 1997). *Cibicides lobatulus* is absent in the sample with *Chilostomella* and *Globobulimina* spp. and its abundance then rises (~30%), suggesting that it could be in situ. Not expected to thrive in deltaic or shoreface environments are *C. kullenbergi*, *P. ariminensis*, *U. rutila*, *C. pseudoungerianus, C. ungerianus* and *S. bulloides*; this would imply that together with the Miocene planktic foraminifera, these outer neritic to bathyal benthic foraminifera are reworked.

Assuming that other species (e.g., *S. deperdita*, *Elphidium* spp., *P. bulloides*, *P. quinqueloba*, *Lenticulina* spp., *Cassidulina* spp.) may be in situ, this benthic foraminifer assemblage is in agreement with shallow, high-energy environments. Several opportunistic taxa feeding on fresh phytodetritus indicate episodes of intermittent, seasonal supply of organic matter. Among these are *Valvulineria* spp. including *V. bradyana* (Amorosi et al., 2013; Goineau et al., 2015 and references therein). A maximum abundance of 30% *E. trinacia* occurs at ±1.5 m and is here apparently not associated with repopulation. Apart from *C. refulgens* and *C. lobatulus*, living attached to hard substrates, the taxa assumed to be in situ are epifaunal and shallow infaunal and indicate a generally more oligo- to mesotrophic, hypoxic environment towards the top of the sampled section (e.g., Jorissen, 1987; Kaiho, 1999; Murray, 2006). In such an environment, specimens of the ostracod *Cyprideis* sp., usually regarded as a brackish species (Benson, 1978), are also considered reworked.

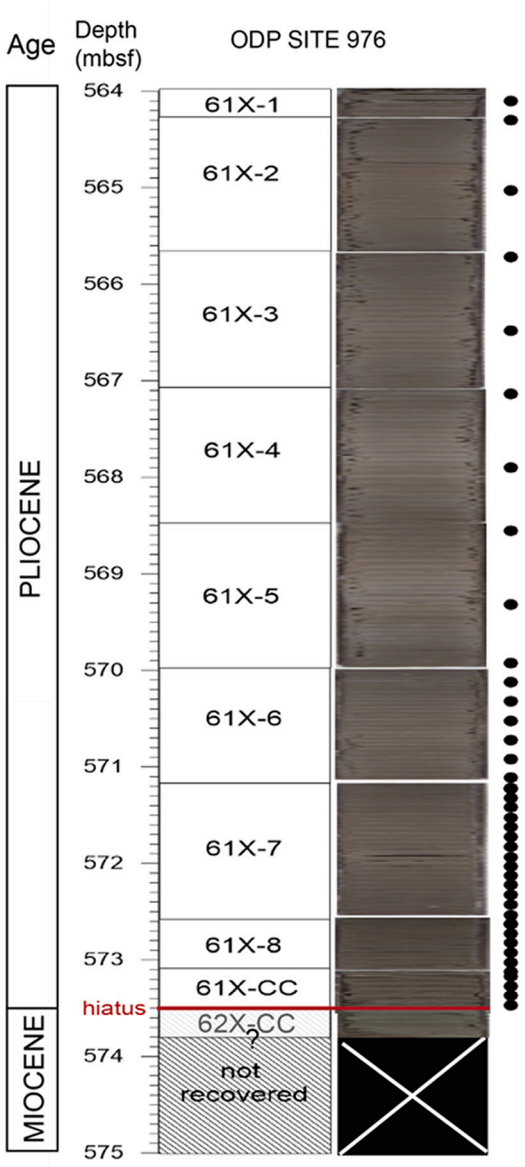

Fig. 7. Early Pliocene core sections from ODP Site 976 with corresponding core photographs. The black dots represent the analysed samples.

5.3.1.3. Zorreras section (Sorbas Basin). In the Zorreras section, where the upper Messinian is continental, the lowermost Pliocene sediments consist of clastic sands with scarce low-diverse benthic foraminifera and no repopulation sequence is found. The first species appearing in the grey layer is monospecific *N. fabum*, included in the shallow infauna group, which is in the Rio Mendelin section the dominant species immediately following the level with monospecific *E. trinacria.* Here, the presence of numerous calcareous nodules, together with *N. fabum* known to tolerate shallow inner shelf environments and eutrophic conditions (Fontanier et al., 2002; Murray, 2006; Duchemin et al., 2008), indicate that the palaeoenvironment was not permanently submerged, but marine water could have intermittently entered the basin through a local geological barrier. While *N. fabum* dominates the entire section, at 1.1 and 1.2 m above the base of the Pliocene some *Elphidium* spp. and rare *C. lobatulus* appear. Together this suggests a gradual ingression of marine waters and a nearshore marine environment which was permanently established after the transgressive pulse that deposited the 5-cm thick bivalve-rich horizon.

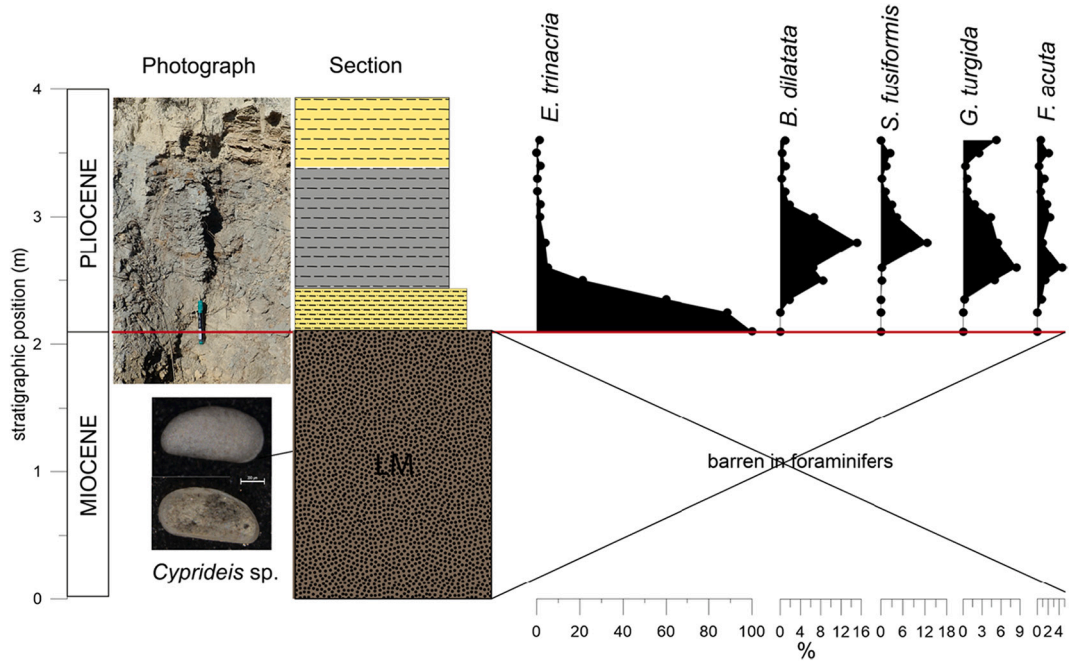

Fig. 8. Base of the Rio Mendelin section. From left to right: the photo of the Miocene-Pliocene boundary (red line), the stratigraphic section and the first benthic foraminiferal species that repopulate early Pliocene environments. In addition, a photo of the predominant late Messinian ostracod species *Cyprideis* sp. is shown. (For interpretation of the references to colour in this figure legend, the reader is referred to the web version of this article.)

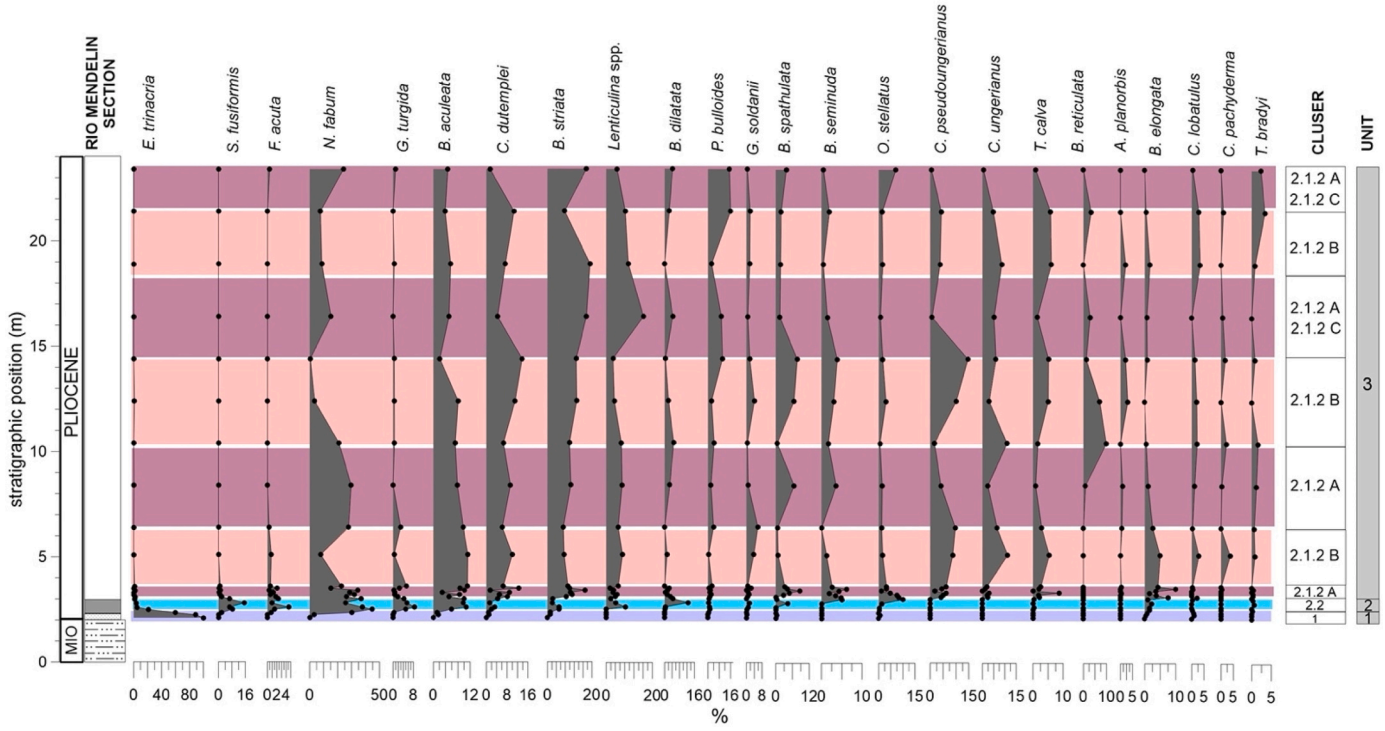

Fig. 9. Variations in relative abundances of major benthic foraminiferal taxa of the Rio Mendelin section. Colour bands correspond to foraminiferal assemblages characterizing the sample clustering in Fig. 10 which was the basis for the definition of micropaleontological units.

5.3.2. Deep basin: ODP Site 976 (Alboran Basin)

The lowermost Pliocene Unit 1 at ODP Site 976 may not cover the MPB because there is an interval of non-recovery in core 62, right below the first Pliocene sediments (Fig. 7) and a black or grey layer is absent. However, a relatively diverse planktic assemblage is present from the base of the studied interval (core 61×-CC, 573.5 mbsf: Fig. 7), with *G. margaritae* and *Sphaeroidinellopsis* spp. appearing at 572.6 m and 572.3 m respectively (Supp. 1). In addition, an interval with high abundances of *U. peregrina* (Fig. 13) was also identified in other deep sites (from cycle 6 to 10 in Sicily, and from cycle 4 to 12 in the Tyrrhenian Sea). It is referred to as the *Uvigerina pygmea-U. peregrina* event (Sgarrella et al., 1997; Barra et al., 1998; Iaccarino et al., 1999b) and has

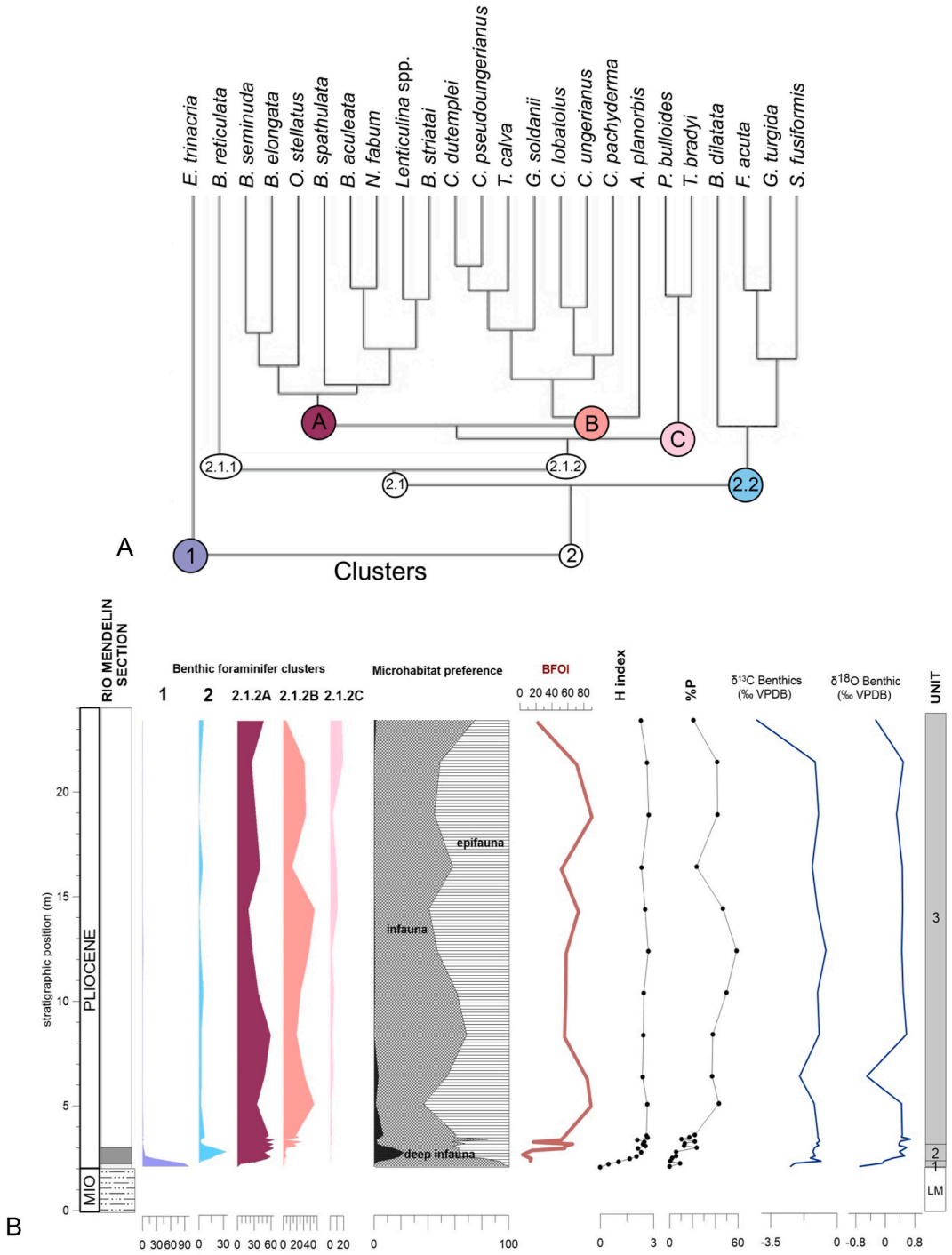

Fig. 10. A) Dendrogram resulting from the hierarchical clustering in the Rio Mendelin section. The clusters have been highlighted with colours. For explanation see text. B) from left to right: Clusters 1, 2.2, 2.1.2 A, 2.1.2 B and 2.1.2C plotted against stratigraphic position; Microhabitat distribution of the most abundant benthic foraminifer species; The BFOI estimation (Kaiho, 1994); Shannon diversity index; % of planktic foraminifera; Benthic $\delta^{13}C$ and $\delta^{18}O$ isotopic record (*C. ungerianus*); The column to the right shows the micropalaeontologically defined stratigraphic units based on the cluster analysis.

been used to confirm the early Pliocene age of the sediments.

A benthic repopulation sequence comparable to the Rio Mendelin section is not developed at Site 976. Phytodetritus species (episto-minellids, *G. subglobosa,* small *Gyroidina* spp.) and deep infaunal taxa (e. g., *Chilostomella* and *Globobulimina* spp.; Jorissen, 1999) each amount to not >5%. Instead, Unit 1 is characterised by a single peak of *B. aculeata* (>35%), with *C. dutemplei* (6%) forming Cluster 1 (Figs. 13 and 14). *Bulimina aculeata* is one of the most opportunistic taxa in the Mediterranean (De Rijk et al., 2000), feeding on fresh phytodetritus and tolerating suboxic environments (Schnitker, 1993; Gebhardt, 1999). *Cibicides dutemplei* is generally assumed to tolerate little oxygen deficiency, although *Cibicides* spp. have been observed in oxygen-deficient environments as well but they may be more sensitive to fresh (undegraded) food particles than to hypoxia (Jorissen et al., 2007). Considering that the abundance peak of *B. aculeata* co-occurs with stress-tolerant species such as *M. barleeanum*, *M. soldanii* (Caralp, 1989; Koho et al., 2008), and *Lenticulina* spp. (Sen Gupta and Machain-Castillo, 1993; Kaiho, 1994) the basal Pliocene bottom-water environment of Site

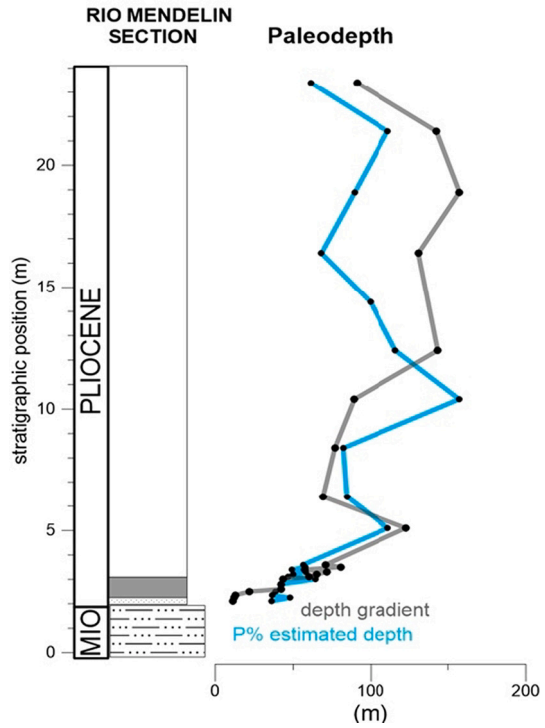

Fig. 11. Calculated palaeodepths for the Rio Mendelin section. The grey line is the palaeodepth estimated by gradient analysis (Hohenegger, 2005; Hohenegger et al., 2008). The blue line is the palaeodepth estimated by using the %P (Van der Zwaan et al., 1990). (For interpretation of the references to colour in this figure legend, the reader is referred to the web version of this article.)

976 was probably characterised by seasonal organic carbon supply and reduced oxygen levels, in agreement with the BFOI values indicative of low-oxic environments (~20, Fig. 14).

Unit 2 is still dominated by infaunal, low-oxic taxa. The appearance of the benthic foraminiferal assemblage of Unit 3 (Figs. 13 and 14) and the decline in abundances of taxa present in Units 1 and 2 reflects a change in environmental conditions. Taxa increasing in abundance include *G. subglobosa* (up to 40%) and later *U. peregrina* (up to 30%; Cluster 2.2.1; Fig. 14). Although shallow infaunal taxa are still dominating the assemblage and the diversity (H index) does not increase, the BFOI rises from a mean of 40 to a mean of 80 (Fig. 14), suggesting the presence of well oxygenated waters. Dominance of *G. subglobosa* (in size fractions >150 μm and 63–150 μm) has been recorded in the oxygen minimum zone (OMZ) of the Sulu Sea, under high fluxes of organic matter (e.g., Miao and Thunell, 1993), but *G. subglobosa* is also a phytodetritus feeder in the generally oxic and oligotrophic environments of the Porcupine Abyssal Plain where the spring bloom delivers pulsed supply of fresh organic matter (Gooday, 1993). It is also present in moderately dysaerobic environments characterised by efficient preservation of organic matter (Loubère et al., 1988) as well as in early Pliocene recolonization successions (Barra et al., 1998). *Uvigerina peregrina* is a shallow infaunal species associated with upwelling and labile (fresh) organic material, and generally not associated with low-oxygen conditions (Morigi et al., 2001; Fontanier et al., 2002; Koho et al., 2008; Schmiedl et al., 2010).

Other species in this assemblage include *S. bulloides* and *B. striata*, indicating upwelling and an elevated organic carbon content (Sen Gupta and Machain-Castillo, 1993; Licari and Mackensen, 2005). *Cibicidoides pachyderma* and *P. ariminensis* generally live in well-oxygenated environments (Schmiedl et al., 2000; Schmiedl et al., 2003), although they also tolerate oxygen deficiency and sustained organic matter fluxes (Bernhard and Gupta, 1999). The benthic foraminiferal assemblage reflects better circulation and installation of an upwelling regime. The change towards higher and more stable BFOI (~80–95) suggest a progressive increase in oxygen levels.

From 569 mbsf, the Cluster 2.2.2 assemblage returns (Fig. 14 and Supp. 2), with a maximum abundance of *M. barleeanus* (25%) at the base and with additional presence of *C. oblongus* and *A. helicinus* (Cluster 2.1). *Anomalinoides helicinus* indicates increased productivity and/or preservation of organic matter (Barra et al., 1998) and *C. oblongus* can also be related to high organic flux and lower oxygen (Murray, 2006). Considering the high BFOI values (~ 50–60), bottom water oxygen levels must have been quite high, even if slightly decreasing from this point onward towards low oxic conditions.

Despite differences, repopulation of the early Pliocene bottom-water environments at deep Mediterranean sites has elements in common. The earliest Pliocene is characterised by the presence of phytodetritus feeders at Site 975 and Eraclea Minoa (e.g., *Eponides pusillus* and *Epistominella exigua*) and contains shallow infaunal species at Sites 976 and 975 (e.g., *Bulimina* spp. and *Bolivina* spp.). All sites are characterised in the early Zanclean by reduced oxygen and high organic flux. After this first interval, all sites are characterised by a gradual amelioration of circulation leading to better oxygenated, and in Eraclea Minoa to fully

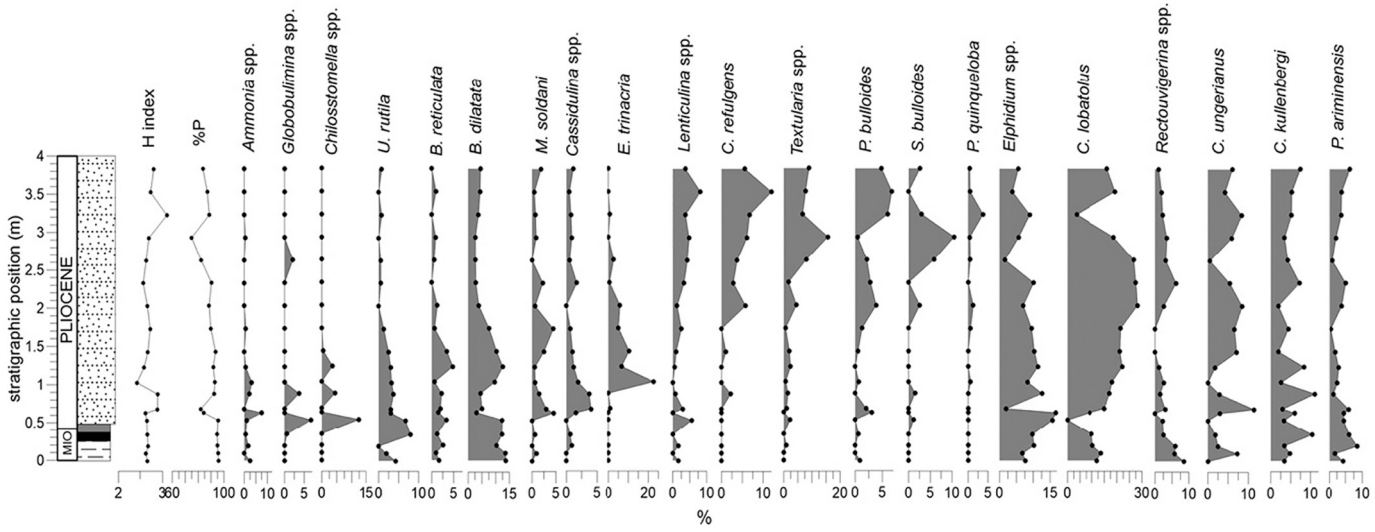

Fig. 12. The Barranco del Negro section with from left to right: the Shannon diversity index, the % of planktic foraminifera, benthic foraminifer per gram and the variations in relative abundances of most abundant benthic foraminiferal taxa are shown.

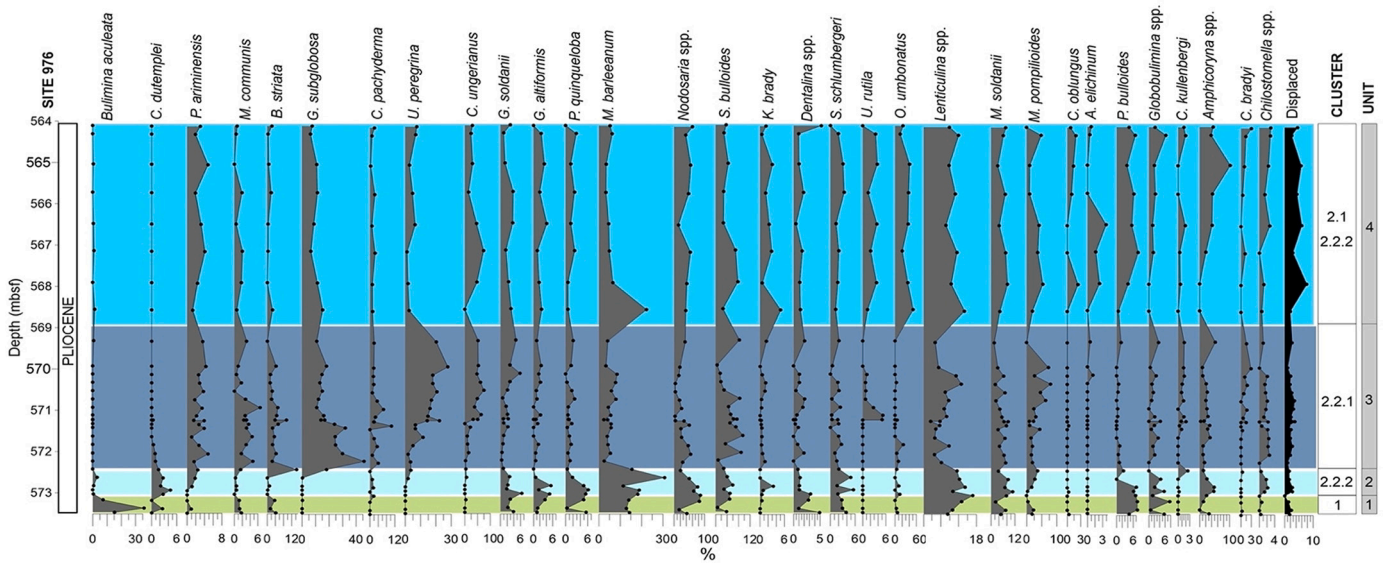

Fig. 13. ODP Site 976: Variations in relative abundances of major benthic foraminiferal taxa. Colour bands correspond to foraminiferal assemblages associated with the clusters of the dendrogram (Fig. 14) and Units 1–4.

open marine conditions.

5.4. *Efficiency of the early Pliocene Mediterranean – Atlantic connections*

In order to better understand Mediterranean-Atlantic connectivity changes at the onset of the Pliocene as well as salinity and temperature differences between the Mediterranean and Atlantic, the newly acquired early Pliocene benthic $\delta^{13}C$ and $\delta^{18}O$ isotopic records from Site 976 and the Rio Mendelin section have been compared with ODP Site 982 (Hodell et al., 2001; Drury et al., 2018) and IODP Site U1387 (Hernández-Molina et al., 2013; Van Der Schee et al., 2016; Figs. 16 and 17). Site U1387 is located in the Gulf of Cadiz, on the Atlantic side of the Strait of Gibraltar at 559 m water depth (Hernández-Molina et al., 2013), which is bathed today by Mediterranean Outflow Water (MOW). This water mass is composed mainly of Levantine Intermediate Water and a small component of West Mediterranean Deep Water (WMDW) averaging 13 °C and 38.4 psu (Bryden and Stommel, 1984; Bryden et al., 1994; Hernandez-Molina et al., 2014). Site 982 is located in the north Atlantic at a water depth of 1135.3 m (Jansen et al., 1996) and bathed currently by the cold (3–8 °C) and less saline (34.95–35.2 ‰) North Atlantic Deep Water (NADW; Ochoa and Bray, 1991; Venz et al., 1999; Hernández-Molina et al., 2016).

In the areas of deep-water formation, deep-water $\delta^{13}C$ is controlled by the $\delta^{13}C$ of the surface. During photosynthesis, the phytoplankton preferentially extract ^{13}C-depleted CO_2, enriching surface waters with the heavy ^{13}C isotope. In contrast, the degradation of sinking organic matter during deep-water renewal releases ^{13}C depleted CO_2 leading to a progressive decrease of $\delta^{13}C$ in deep-water masses. This decrease depends on the quantity of CO_2 added by remineralization of organic matter, and so, on the deep-water residence time and bottom-water ventilation (Laube-Lenfant and Pierre, 1994; Pierre, 1999).

The early Pliocene benthic $\delta^{13}C$ values at Site 976 are initially analogous to the ones registered at the Gulf of Cadiz (Fig. 16; Site 1387) and become increasingly heavier up core when they reach the Atlantic curve (Site 982), which reflects the well ventilated high $\delta^{13}C$ of the NADW. In contrast, the more depleted Messinian $\delta^{13}C$ values from Site 976 (average value around −1 per mil) reflect the longer bottom-water residence time of Mediterranean caused by the reduced Mediterranean – Atlantic exchange (Bulian et al., 2022). In the Pliocene, with the reestablishment of an efficient Mediterranean – Atlantic water exchange, Site 976 benthic $\delta^{13}C$ rises to Atlantic values. Nonetheless, benthic species present at the base of the Pliocene suggest both reduced oxygen levels and high organic carbon content which is not visible from the benthic $\delta^{13}C$. This discrepancy can be explained by assuming that the high bottom-water renewal rate and DIC (Dissolved Inorganic Carbon) characterised by high $\delta^{13}C$ was not large enough to dramatically reduce the $\delta^{13}C$ at the seafloor, despite high remineralisation rates. Early Pliocene benthic $\delta^{13}C$ values from the marginal Rio Mendelin section are generally lower than Atlantic and Mediterranean values showing a ~ 2 ‰ offset. This suggests that while the deep Mediterranean was efficiently connected with the Atlantic, this marginal basin could have still been isolated from the Mediterranean.

The $\delta^{18}O$ values for the early Pliocene in the marginal Rio Mendelin section and deep ODP Site 976 are very similar and most probably reflect a comparable temperature and salinity (Fig. 17). At the same time, lighter Mediterranean, and heavier Gulf of Cadiz (Site 1387) values show an offset of almost 2 ‰, which is the opposite situation in comparison with the present one (Fig. 17). As a reference for the latest Holocene data, we used the *Cibicidoides pachyderma* benthic $\delta^{18}O$ values recorded in the Alboran Sea (Pérez-Asensio et al., 2020) and Gulf of Cadiz Site 1387 (Singh et al., 2015). To these data we applied a correction of −0.25 ‰ accounting for the difference in ice volume between the early Pliocene and the late Holocene (Raymo et al., 2018). From this comparison it emerged that the present day $\delta^{18}O$ difference between IODP site U1387 in the Gulf of Cadiz and ODP site 976 in the Alboran Sea is −0.75 ‰ (Fig. 17, dashed lines). This difference is probably due to the higher $\delta^{18}O$ of Mediterranean waters due to its negative water budget and higher salinities compared to those of the Atlantic. However, in the early Pliocene we observe an opposite benthic $\delta^{18}O$ offset between the Gulf of Cadiz and Alboran, which was ~ +1.75 ‰. If the large positive Pliocene offset was due to temperature alone, there would have been an 8 °C difference between Mediterranean and Atlantic deep waters on both sides of the Strait (0.23 ‰ = 1 °C), while this difference today is only 1–3 °C (MEDARGroup, 2002). This suggests that at the depth of Site U1387 the thermal influence of the MOW was low during the early Pliocene, which could be explained if the flow of warm Mediterranean waters to the Atlantic was lower than today. A lower flow of heat from the Mediterranean to the Atlantic would have increased the temperature difference between the two basins and consequently the oxygen isotope difference. Another scenario that could justify such Pliocene offset between the benthic $\delta^{18}O$ in the Alboran Sea and the Gulf of Cadiz is that Mediterranean seawater salinity and $\delta^{18}O$

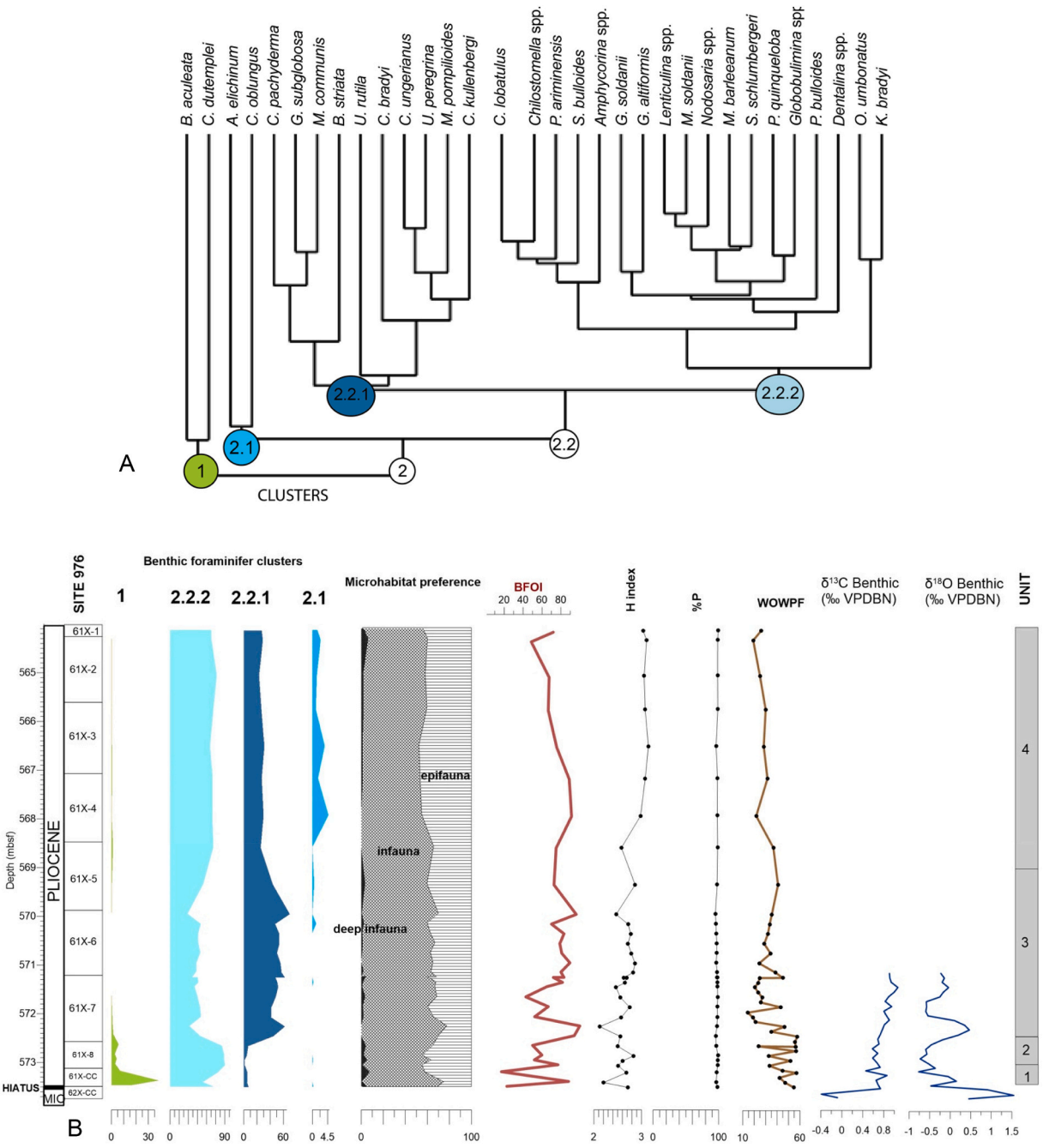

Fig. 14. ODP Site 976: A) Dendrogram resulting from the hierarchical clustering that divided the benthic foraminifer species in two main species clusters (Cluster 1, Cluster 2) and two subclusters (Clusters 2.1 and 2.2). Cluster 2.2 in turn branches to two subordinate branches as well (Cluster 2.2.1 and 2.2.2). The used clusters have been highlighted with specific colours. B) From left to right: Clusters 1, 2.1, 2.2.1 and 2.2.2 plotted against stratigraphic position; Microhabitat distribution of the most abundant benthic foraminifer species; The BFOI estimation (Kaiho, 1994); Shannon diversity index; % of planktic foraminifers; Benthic $\delta^{13}C$ and $\delta^{18}O$ isotopic record (*C. pachyderma*); The column of the right contains the micropaleontologically defined stratigraphic units based on the cluster analysis.

were lower than today and/or that the Strait was much wider than today. This would imply that in the earliest Pliocene the Mediterranean water budget would have been less negative than today, or even positive. Lower salinities agree with the latest Messinian scenario, where the Mediterranean water would contain a strong Paratethyan signal which was partly maintained through the early Pliocene as well. A much wider strait in the early Pliocene compared to the present would have exposed the Mediterranean water for a shorter time to a negative water budget, resulting in lower $\delta^{18}O$ and salinities of Mediterranean water.

Even more extreme is the offset between the Mediterranean benthic $\delta^{18}O$ and Atlantic Site 982 record. This offset is probably due to the difference in temperature between these two water masses. Today, the Mediterranean deep-water temperature is in the order of 13 °C, while deep water temperature at the location of site 982 is close to 4–5 °C (MEDARGroup, 2002). This different water temperature would result in a $\delta^{18}O$ offset of 2 ‰, which is still lower than the observed $\delta^{18}O$ difference in the early Pliocene between site 976 and 982. This could be explained again by the occurrence of lighter $\delta^{18}O$ waters in the deep Mediterranean probably due to a less negative water budget during the early Pliocene.

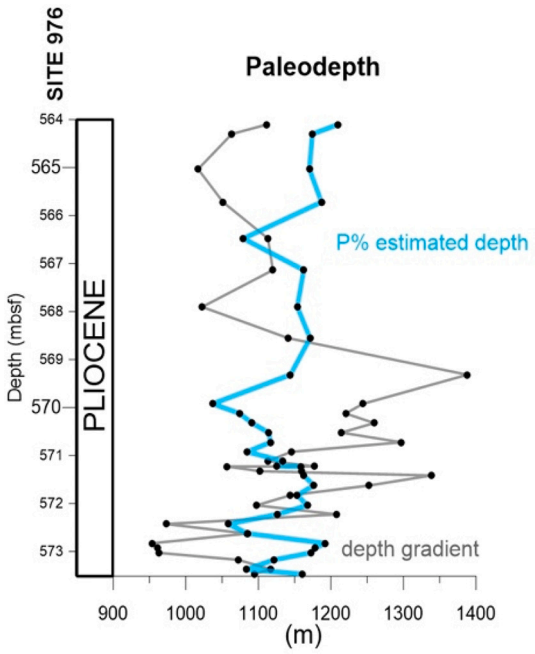

Fig. 15. Calculated palaeodepths for ODP Site 976. The grey line is the palaeodepth estimated by gradient analysis (Hohenegger, 2005; Hohenegger et al., 2008). The blue line is the palaeodepth estimated by using the %P (Van der Zwaan et al., 1990). (For interpretation of the references to colour in this figure legend, the reader is referred to the web version of this article.)

6. Conclusions

The studied upper Messinian–lower Pliocene sections in the Spanish basins reflect the sedimentological changes linked with the reestablishment of normal marine conditions after the MSC and give important information about the water level across the Miocene-Pliocene boundary.

In the marginal sections (Rio Mendelin, Barranco del Negro, Zorreras), the earliest Pliocene sediments show as a dark layer, usually grey or black, often enriched in organic matter. This layer, identified in deep and marginal basins all over the Mediterranean, could imply water column stratification, and reduced bottom-water oxygen levels, which is in agreement with the benthic foraminiferal assemblages. Such conditions could develop in a scenario where the Atlantic inflow reaching the Mediterranean was more saline than the Mediterranean waters still under the influence of the Paratethys, causing Atlantic waters to sink and stratify the water column. The early Pliocene of ODP Site 976 located in the Alboran Basin does not show a dark layer, probably because of its proximity to the Strait of Gibraltar and the inflowing Atlantic waters that could have eroded the basal Pliocene layers.

The analyses performed on benthic foraminiferal assemblages enable a more detailed reconstruction of the early Pliocene Mediterranean environments and reflect benthic foraminiferal repopulation of the sea floor. The first benthic faunas that appear are in line with reduced bottom-water oxygen levels and a stratified water column in agreement with the deposition of the dark layers at the MPB. During the early Pliocene, the sea-level rise re-established normal marine conditions in the Mediterranean as can be deduced from the benthic foraminiferal assemblages characterizing this interval. The benthic foraminiferal repopulation identified in the studied basins is comparable with other Mediterranean sections and cores and shows similarities with repopulation following sapropel deposition. The general repopulation trend shows a shift from stressed and unstable environments to benthic assemblages indicating an amelioration of the circulation and bottom-water oxygenation.

In the studied marginal Spanish basins, the estimated palaeobathymetry for the early Pliocene was similar ranging between 50 and 150 m. In the Malaga Basin, the earliest Pliocene palaeodepth does not exceed 50 m, and eventually reaches values of 150 m. In the Nijar Basin, the presence of macrofossils and fossil traces suggests high-energy shallow environments just after the MPB, while towards the top of the sections deeper, less high-energy environments were probably established. These observations imply a progressive deepening of the Mediterranean marginal basins as the Mediterranean – Atlantic connectivity was becoming more efficient. At Site 976, the early Pliocene is characterised by a bathyal environment (>1000 m), which is within the range we find today.

Although the water column may have been stratified and organic matter accumulating, the high $\delta^{13}C$ values from Site 976 testify that

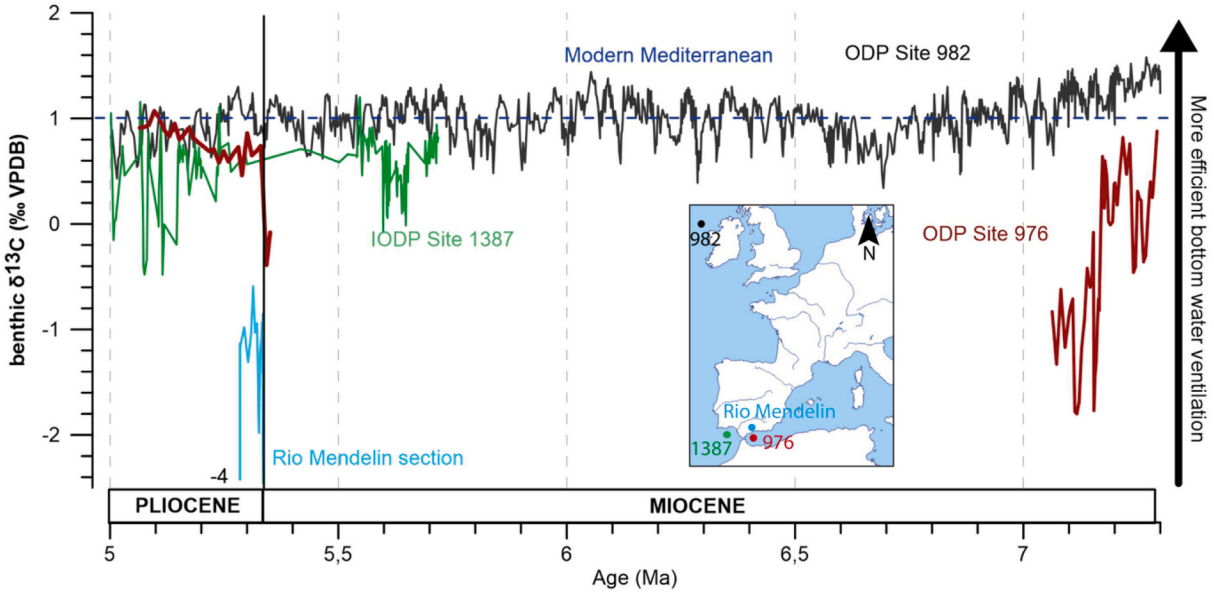

Fig. 16. Comparison between benthic $\delta^{13}C$ records of Site 976 and the Rio Mendelin section (this study) with Atlantic Ocean ODP Site 982 (Hodell et al., 2001; Drury et al., 2018) and IODP Site 1387 (Van Der Schee et al., 2016). The blue dashed line shows modern Mediterranean benthic $\delta^{18}O$ values (Pérez-Asensio et al., 2020). The map shows the locations of the sites. (For interpretation of the references to colour in this figure legend, the reader is referred to the web version of this article.)

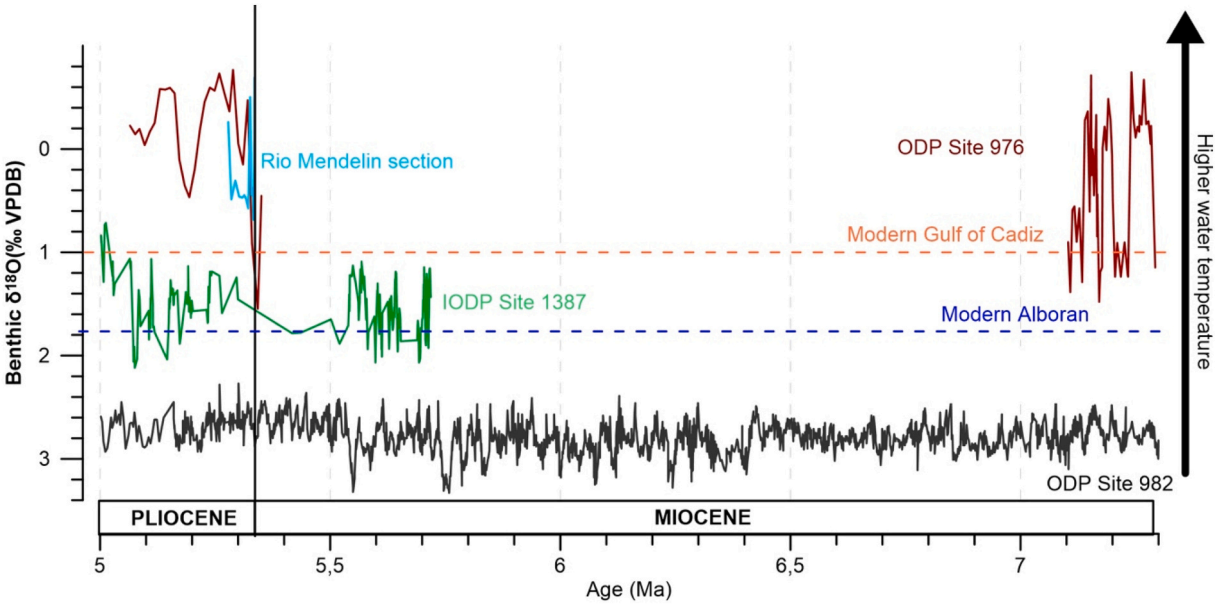

Fig. 17. Comparison between benthic $\delta^{18}O$ records of Site 976 and the Rio Mendelin section (this study) with Atlantic Ocean ODP Site 982 (Drury et al., 2018) and IODP Site 1387 (Van Der Schee et al., 2016). The blue dashed line shows modern Mediterranean benthic $\delta^{18}O$ values (Pérez-Asensio et al., 2020). The orange dashed line refers to the modern Gulf of Cadiz values (Singh et al., 2015). Both are corrected with respect to the Raymo et al. (2018) global curve. (For interpretation of the references to colour in this figure legend, the reader is referred to the web version of this article.)

bottom-water renewal in the deep basins was efficient immediately after the reflooding and that an efficient basin-scale circulation was re-established. The values are in fact almost 2‰ higher than the ones registered in concomitance with the first gateway restriction at 7.17 Ma.

The significant offset between the Alboran Basin and Gulf of Cadiz benthic $\delta^{18}O$ values for the early Pliocene can be related either to a temperature or salinity difference among the two basins. However, because of the opposite isotopic offset between the benthic $\delta^{18}O$ in the early Pliocene and late Holocene we believe that the Pliocene water budget was less negative than today, rendering the difference in salinity between the two basins the prevailing factor determining the $\delta^{18}O$. A less saline early Pliocene Mediterranean is in line with continuation of the Paratethyan influence present in the latest Messinian, and consequently with stratification of the water column once the Atlantic waters invaded the basin.

CRediT authorship contribution statement

F. Bulian: Conceptualization, Investigation, Methodology, Data curation, Writing – original draft. **T.J. Kouwenhoven:** Methodology, Data curation, Supervision, Writing – review & editing. **N. Andersen:** Formal analysis, Writing - review & editing. **W. Krijgsman:** Resources, Conceptualization, Supervision, Writing – review & editing. **F.J. Sierro:** Resources, Conceptualization, Supervision, Writing – review & editing.

Declaration of Competing Interest

The authors declare that they have no known competing financial interests or personal relationships that could have appeared to influence the work reported in this paper.

Acknowledgments

The authors appreciate the work of Jose Ignacio Martin Cruz in sample processing and preparation. Robert Speijer is thanked for his input when classifying benthic foraminiferal species and Federico Andreetto for his advice regarding ostracod identification. We also appreciate the useful information on outcrop location provided by Frits Hilgen. Moreover, all fellow ESRs and supervisors from the SALTGIANT project are thanked for their valuable suggestions and discussions. A part of the samples used in this research were collected through ODP Expedition 161 aboard the Joides Resolution. This research has received funding from the European Union's Horizon 2020 research and innovation program under the Marie Skłodowska-Curie grant agreement n° 765256 SALTGIANT.

Appendix A. Supplementary data

Supplementary data to this article can be found online at https://doi.org/10.1016/j.marmicro.2022.102160.

References

Aguirre, J., 1998. El Plioceno del SE de la Península Ibérica (provincia de Almería). Síntesis estratigráfica, sedimentaria, bioestratigráfica y paleogeográfica. Rev. Soc. Geol. Esp. 11 (3), 297–316.
Aguirre, J., Sánchez-Almazo, I.M., 2004. The Messinian post-evaporitic deposits of the Gafares area (Almería-Níjar basin, SE Spain). A new view of the "Lago-Mare" facies. Sediment. Geol. 168 (1–2), 71–95.
Aguirre, J., Pérez-Muñoz, A., Sanchez-Almazo, I., 2006. Benthic foraminifer assemblages in the lower Pliocene deposits of the Almeria-Níjar Basin (SE Spain). Rev. Esp. Micropaleontol. 38 (2), 411–428.
Alve, E., 2003. A common opportunistic foraminiferal species as an indicator of rapidly changing conditions in a range of environments. Estuar. Coast. Shelf Sci. 57 (3), 501–514.
Amorosi, A., Rossi, V., Vella, C., 2013. Stepwise post-glacial transgression in the Rhône Delta area as revealed by high-resolution core data. Palaeogeogr. Palaeoclimatol. Palaeoecol. 374, 314–326.
Andreetto, F., Aloisi, G., Raad, F., Heida, H., Flecker, R., Agiadi, K., Lofi, J., Blondel, S., Bulian, F., Camerlenghi, A., 2021a. Freshening of the Mediterranean Salt Giant: controversies and certainties around the terminal (Upper Gypsum and Lago-Mare) phases of the Messinian Salinity Crisis. Earth Sci. Rev. 103577.
Andreetto, F., Matsubara, K., Beets, C., Fortuin, A., Flecker, R., Krijgsman, W., 2021b. High Mediterranean water-level during the Lago-Mare phase of the Messinian Salinity Crisis: insights from the Sr isotope records of Spanish marginal basins (SE Spain). Palaeogeogr. Palaeoclimatol. Palaeoecol. 562, 110139.
Anthony, E.J., Aagaard, T., 2020. The lower shoreface: Morphodynamics and sediment connectivity with the upper shoreface and beach. Earth Sci. Rev. 103334.
Aufgebauer, A., McCann, T., 2011. Messinian to Pliocene transition in the deep part of the Sorbas Basin, SE Spain—A new description of the depositional environment during the Messinian Salinity Crisis.(With 8 figures and 1 table). Neues Jah. Geol. Palaontol. Abh. 259 (2), 177.
Austin, W., Evans, J., 2000. NE Atlantic benthic foraminifera: modern distribution patterns and palaeoecological significance. J. Geol. Soc. 157 (3), 679–691.

Avnaim-Katav, S., Milker, Y., Schmiedl, G., Sivan, D., Hyams-Kaphzan, O., Sandler, A., Almogi-Labin, A., 2016. Impact of eustatic and tectonic processes on the southeastern Mediterranean shelf during the last one million years: Quantitative reconstructions using a foraminiferal transfer function. Mar. Geol. 376, 26–38.
Bache, F., Popescu, S.M., Rabineau, M., Gorini, C., Suc, J.P., Clauzon, G., Olivet, J.L., Rubino, J.L., Melinte-Dobrinescu, M.C., Estrada, F., Londeix, L., Armijo, R., Meyer, B., Jolivet, L., Jouannic, G., Leroux, E., Aslanian, D., Reis, A.T.D., Mocochain, L., Dumurdžanov, N., Zagorchev, I., Lesić, V., Tomić, D., Namik Çağatay, M., Brun, J.P., Sokoutis, D., Csato, I., Ucarkus, G., Çakir, Z., 2012. A two-step process for the reflooding of the Mediterranean after the Messinian Salinity Crisis. Basin Res. 24 (2), 125–153.
Bache, F., Gargani, J., Suc, J.P., Gorini, C., Rabineau, M., Popescu, S.M., Leroux, E., Couto, D.D., Jouannic, G., Rubino, J.L., Olivet, J.L., Clauzon, G., Dos Reis, A.T., Aslanian, D., 2015. Messinian evaporite deposition during sea level rise in the Gulf of Lions (Western Mediterranean). Mar. Pet. Geol. 66, 262–277.
Baggley, K.A., 2000. The Late Tortonian-Early Messinian Foraminiferal record of the Abad Member (Turre Formation), Sorbas Basin, Almería, South-East Spain. Palaeontology 43 (6), 1069–1112.
Baldi, K., Hohenegger, J., 2008. Paleoecology of benthic foraminifera of the Baden-Sooss section (Badenian, Middle Miocene, Vienna Basin, Austria). Geol. Carpath. 59 (5), 411–424.
Bandy, O.L., Chierici, M.A., 1966. Depth-temperature evaluation of selected California and Mediterranean bathyal foraminifera. Mar. Geol. 4 (4), 259–271.
Barbieri, R., Panieri, G., 2004. How are benthic foraminiferal faunas influenced by cold seeps? Evidence from the Miocene of Italy1. Palaeogeogr. Palaeoclimatol. Palaeoecol. 204 (257), 275.
Barra, D., Bonaduce, G., Sgarrella, E., 1998. Paleoenvironmental bottom water conditions in the early Zanclean of the Capo Rossello area (Agrigento, Sicily). Bol. Soc. Paleontol. Ital. 37, 61–88.
Bassetti, M.A., Miculan, P., Sierro, F.J., 2006. Evolution of depositional environments after the end of Messinian Salinity Crisis in Nijar basin (SE Betic Cordillera). Sediment. Geol. 188, 279–295.
Benson, R.H., 1978. 35. The paleoecology of the ostracodes of DSDP Leg 42A. In: Hsü, K. J., Montadert, L., Bernoulli, D., Bizon, G., Cita, M., Erickson, A., Fabricius, F., Garrison, R.E., Kidd, R.B., Mélières, F., Müller, C., Wright, R.C. (Eds.), Initial Reports of the Deep Sea Drilling Project, Washington DC, 42(part 1), pp. 777–786.
Berggren, W., Haq, B.U., 1976. The Andalusian stage (late Miocene): biostratigraphy, biochronology and paleoecology. Palaeogeogr. Palaeoclimatol. Palaeoecol. 20 (1–2), 67–129.
Bernhard, J.M., Gupta, B.K.S., 1999. Foraminifera of oxygen-depleted environments. In: Modern Foraminifera. Springer, pp. 201–216.
Bizon, G., Bizon, J., 1984. Distribution des foraminifères sur le plateau continental au large du Rhône. In: Ecologie des microorganismes en Méditerranée occidentale 'ECOMED'. Association Française des Techniciens du Pétrole, Paris, pp. 84–94.
Blanc, P.-L., 2002. The opening of the Plio-Quaternary Gibraltar Strait: assessing the size of a cataclysm. Geodin. Acta 15 (5–6), 303–317.
Brolsma, M.J., 1978. Quantitative Forminiferal Analysis and Environmental Interpretation of the Pliocene and Topmost Miocene on the South Coast of Sicily. Utrecht University.
Bryden, H., Stommel, H., 1984. Limiting processes that determine basic features of the circulation in the Mediterranean-Sea. Oceanol. Acta 7 (3), 289–296.
Bryden, H.L., Candela, J., Kinder, T.H., 1994. Exchange through the Strait of Gibraltar. Prog. Oceanogr. 33 (3), 201–248.
Bulian, F., Sierro, F.J., Ledesma, S., Jiménez-Espejo, F.J., Bassetti, M.-A., 2021. Messinian West Alboran Sea record in the proximity of Gibraltar: early signs of Atlantic-Mediterranean gateway restriction. Mar. Geol. 106430.
Bulian, F., Kouwenhoven, T.J., Jiménez-Espejo, F.J., Krijgsman, W., Andersen, N., Sierro, F.J., 2022. Impact of the Mediterranean-Atlantic connectivity and the late Miocene carbon shift on deep-sea communities in the Western Alboran Basin. Palaeogeogr. Palaeoclimatol. Palaeoecol. 110841.
Caralp, M.H., 1989. Size and morphology of the benthic foraminifer Melonis barleeanum; relationships with marine organic matter. J. Foraminifer. Res. 19 (3), 235–245.
Caruso, A., Blanc-Valleron, M.-M., Da Prato, S., Pierre, C., Rouchy, J.M., 2020. The late Messinian "Lago-Mare" event and the Zanclean Reflooding in the Mediterranean Sea: new insights from the Cuevas del Almanzora section (Vera Basin, South-Eastern Spain). Earth Sci. Rev. 200, 102993.
CIESM, 2008. The Messinian salinity crisis from mega-deposits to microbiology. In: Briand, F. (Ed.), A consensus report, in 33ème CIESM Workshop Monographs, 33. CIESM, 16, bd de Suisse, MC-98000, Monaco, pp. 1–168.
Cipollari, P., Cosentino, D., Radeff, G., Schildgen, T.F., Faranda, C., Grossi, F., Gliozzi, E., Smedile, A., Gennari, R., Darbaş, G., 2013. Easternmost Mediterranean evidence of the Zanclean flooding event and subsequent surface uplift: Adana Basin, southern Turkey. Geol. Soc. Lond., Spec. Publ. 372 (1), 473–494.
Cita, M., Zocchi, M., 1978. Distribution patterns of benthic foraminifera on floor of Mediterranean Sea. Oceanol. Acta 1 (4), 445–462.
Cita, M.B., Wright, R.C., Ryan, W.B.F., Longinelli, A., 1978. Messinian paleoenvironments. In: Hsü, K.J., Montadert, L., et al. (Eds.), Init. Rep. D.S.D.P., vol. 42A. US Government Printing Office, Washington, pp. 1003–1035.
Comas, M.C., Zahn, R., Klaus, A., et al., 1996. ODP, Init. Repts., 161: College Station, TX (Ocean Drilling Program).
Corbí, H., 2010. Los foraminíferos de la cuenca neógena del Bajo Segura (sureste de España): bioestratigrafía y cambios paleoambientales en relación con la Crisis de Salinidad del Mediterráneo. Tesis doctorales.
Corbí, H., Soria, J.M., 2016. Late Miocene–early Pliocene planktonic foraminifer event-stratigraphy of the Bajo Segura basin: a complete record of the western Mediterranean. Mar. Pet. Geol. 77, 1010–1027.
Corliss, B.H., Chen, C., 1988. Morphotype patterns of Norwegian Sea deep-sea benthic foraminifera and ecological implications. Geology 16 (8), 716–719.
Cornée, J.-J., Münch, P., Achalhi, M., Merzeraud, G., Azdimousa, A., Quillévéré, F., Melinte-Dobrinescu, M., Chaix, C., Moussa, A.B., Lofi, J., 2016. The Messinian erosional surface and early Pliocene reflooding in the Alboran Sea: New insights from the Boudinar basin, Morocco. Sediment. Geol. 333, 115–129.
Dabrio, C.J., Esteban, M., Martin, J.M., 1981. The coral reef of Nijar, Messinian (uppermost Miocene), Almeria Province, SE Spain. J. Sediment. Res. 51 (2), 521–539.
De Rijk, S., Troelstra, S., Rohling, E., 1999. Benthic foraminiferal distribution in the Mediterranean Sea. J. Foraminifer. Res. 29 (2), 93–103.
De Rijk, S., Jorissen, F., Rohling, E., Troelstra, S., 2000. Organic flux control on bathymetric zonation of Mediterranean benthic foraminifera. Mar. Micropaleontol. 40 (3), 151–166.
De Stigter, H., Jorissen, F., Van der Zwaan, G., 1998. Bathymetric distribution and microhabitat partitioning of live (Rose Bengal stained) benthic foraminifera along a shelf to bathyal transect in the southern Adriatic Sea. J. Foraminifer. Res. 28 (1), 40–65.
Dela Pierre, F., Natalicchio, M., Lozar, F., Bonetto, S.M.R., Carnevale, G., Cavagna, S., Colombero, S., Sabino, M., Violanti, D., 2016. The Northermost Record of the Messinian Salinity Crisis. Piedmont Basin, NW Italy.
Diz, P., Francés, G., Costas, S., Souto, C., Alejo, I., 2004. Distribution of benthic foraminifera in coarse sediments, Ría de Vigo, NW Iberian margin. J. Foraminifer. Res. 34 (4), 258–275.
Do Couto, D., Popescu, S.-M., Suc, J.-P., Melinte-Dobrinescu, M.C., Barhoun, N., Gorini, C., Jolivet, L., Poort, J., Jouannic, G., Auxietre, J.-L., 2014. Lago Mare and the Messinian salinity crisis: evidence from the Alboran Sea (S. Spain). Mar. Pet. Geol. 52, 57–76.
Donovan, S.K., Jones, S.J., King, A.R., Harper, D.A., 2021. Pliocene Trace Fossils from Oyster Substrates in the Nijar Basin, Betic Cordillera, southern Spain. Proceedings of the Geologists' Association.
Droser, M.L., Bottjer, D.J., 1987. Development of Ichnofabric Indices for Strata Deposited in High-Energy Nearshore Terrigenous Clastic Environments.
Drury, A.J., Westerhold, T., Hodell, D., Röhl, U., 2018. Reinforcing the North Atlantic backbone: revision and extension of the composite splice at ODP Site 982. Clim. Past 14 (3), 321–338.
Duchemin, G., Jorissen, F.J., Le Loc'h, F., Andrieux-Loyer, F., Hily, C., Thouzeau, G., 2008. Seasonal variability of living benthic foraminifera from the outer continental shelf of the Bay of Biscay. J. Sea Res. 59 (4), 297–319.
Esteras, M., Izquierdo, J., Sandoval, N., Mamad, A., 2000. Evolución morfológica y estratigráfica pliocuaternaria del umbral de Camarinal (Estrecho de Gibraltar) basada en sondeos marinos. Rev. Soc. Geol. España 13 (3–4), 539–550.
Estrada, F., Ercilla, G., Gorini, C., Alonso, B., Vázquez, J.T., García-Castellanos, D., Juan, C., Maldonado, A., Ammar, A., Elabbassi, M., 2011. Impact of pulsed Atlantic water inflow into the Alboran Basin at the time of the Zanclean flooding. Geo-Mar. Lett. 31 (5–6), 361–376.
Fentimen, R., Lim, A., Rüggeberg, A., Wheeler, A.J., Van Rooij, D., Foubert, A., 2020. Impact of bottom water currents on benthic foraminiferal assemblages in a cold-water coral environment: the Moira Mounds (NE Atlantic). Mar. Micropaleontol. 154, 101799.
Fontanier, C., Jorissen, F., Licari, L., Alexandre, A., Anschutz, P., Carbonel, P., 2002. Live benthic foraminiferal faunas from the Bay of Biscay: faunal density, composition, and microhabitats. Deep-Sea Res. I Oceanogr. Res. Pap. 49 (4), 751–785.
Fortuin, A.R., Krijgsman, W., 2003. The Messinian of the Nijar Basin (SE Spain): sedimentation, depositional environments and paleogeographic evolution. Sediment. Geol. 160 (1–3), 213–242.
Fortuin, A., Kelling, J., Roep, T.B., 1995. The enigmatic Messinian-Pliocene section of Cuevas del Almanzora (Vera Basin, SE Spain) revisited—erosional features and strontium isotope ages. Sediment. Geol. 97 (3–4), 177–201.
Fortuin, A., Krijgsman, W., Hilgen, F., Sierro, F., 2000. Late Miocene Mediterranean desiccation: topography and significance of the'Salinity Crisis' erosion surface on-land in southeast Spain: comment. Sediment. Geol. 133, 167–174.
García-Alix, A., Minwer-Barakat, R., Martín Suárez, E., Freudenthal, M., Aguirre, J., Kaya, F., 2016. Updating the Europe–Africa small mammal exchange during the late Messinian. J. Biogeogr. 43 (7), 1336–1348.
Garcia-Castellanos, D., Estrada, F., Jiménez-Munt, I., Gorini, C., Fernández, M., Vergés, J., De Vicente, R., 2009. Catastrophic flood of the Mediterranean after the Messinian salinity crisis. Nature 462 (7274), 778.
Garcia-Castellanos, D., Micallef, A., Estrada, F., Camerlenghi, A., Ercilla, G., Periáñez, R., Abril, J.M., 2019. The Zanclean megaflood of the Mediterranean–Searching for additional evidence. Earth Sci. Rev. 103061.
García-García, F., Corbí, H., Soria, J., Viseras, C., 2011. Architecture analysis of a river flood-dominated delta during an overall sea-level rise (early Pliocene, SE Spain). Sediment. Geol. 237 (1–2), 102–113.
Gargani, J., Rigollet, C., 2007. Mediterranean Sea level variations during the Messinian salinity crisis. Geophys. Res. Lett. 34 (10).
Gebhardt, H., 1993. Neogene foraminifera from the Eastern Rabat area (Morocco): stratigraphy, palaeobathymetry and palaeoecology. J. African Earth Sci. (and the Middle East) 16 (4), 445–464.
Gebhardt, H., 1999. Middle to Upper Miocene benthonic foraminiferal palaeoecology of the tap Marls (Alicante Province, SE Spain) and its palaeoceanographic implications. Palaeogeogr. Palaeoclimatol. Palaeoecol. 145 (1–3), 141–156.
Gennari, R., Iaccarino, S.M., Di Stefano, A., Sturiale, G., Cipollari, P., Manzi, V., Roveri, M., Cosentino, D., 2008. The Messinian -Zanclean boundary in the Northern Apennine. Stratigraphy 5 (3–4), 307–322.

Gibson, T.G., 1989. Planktonic benthonic foraminiferal ratios: modern patterns and Tertiary applicability. Mar. Micropaleontol. 15 (1–2), 29–52.
Gingras, M.K., Dashtgard, S.E., MacEachern, J.A., Pemberton, S.G., 2008. Biology of shallow marine ichnology: a modern perspective. Aquat. Biol. 2 (3), 255–268.
Goineau, A., Fontanier, C., Mojtahid, M., Fanget, A.-S., Bassetti, M.-A., Berné, S., Jorissen, F., 2015. Live–dead comparison of benthic foraminiferal faunas from the Rhône prodelta (Gulf of Lions, NW Mediterranean): development of a proxy for palaeoenvironmental reconstructions. Mar. Micropaleontol. 119, 17–33.
Gooday, A.J., 1988. A response by benthic foraminifera to the deposition of phytodetritus in the deep sea. Nature 332 (6159), 70–73.
Gooday, A.J., 1993. Deep-sea benthic foraminiferal species which exploit phytodetritus: characteristic features and controls on distribution. Mar. Micropaleontol. 22 (3), 187–205.
Gooday, A.J., 2003. Benthic foraminifera (Protista) as tools in deep-water palaeoceanography: environmental influences on faunal characteristics. Adv. Mar. Biol. 46, 1–90.
Gooday, A.J., Hughes, J.A., 2002. Foraminifera associated with phytodetritus deposits at a bathyal site in the northern Rockall Trough (NE Atlantic): seasonal contrasts and a comparison of stained and dead assemblages. Mar. Micropaleontol. 46 (1–2), 83–110.
Grossi, F., Cosentino, D., Gliozzi, E., 2008. Late Messinian Lago-Mare ostracods and palaeoenvironments of the central and eastern Mediterranean Basin. Bol. Soc. Paleontol. Ital. 47 (2), 131–146.
Guerra-Merchán, A., Serrano, F., Garcés, M., Gofas, S., López Garrido, A., El Kadiri, K., Hlila, R., 2008. Caracterización de la sedimentación Lago Mare (Messiniense terminal) y de la transgresión del comienzo del Plioceno en la cuenca de Málaga (Cordillera Bética). Geogaceta 44, 207–210.
Guerra-Merchán, A., Serrano, F., Garcés, M., Gofas, S., Esu, D., Gliozzi, E., Grossi, F., 2010. Messinian Lago-Mare deposits near the strait of Gibraltar (Malaga basin, S Spain). Palaeogeogr. Palaeoclimatol. Palaeoecol. 285 (3–4), 264–276.
Guerra-Merchán, A., Serrano, F., Hlila, R., El Kadiri, K., de Galdeano, C.S., Garcés, M., 2014. Tectono-sedimentary evolution of the peripheral basins of the Alboran Sea in the arc of Gibraltar during the latest Messinian-Pliocene. J. Geodyn. 77, 158–170.
Haake, F.W., 1982. Occurrences of Living and Dead Salt Marsh Foraminifera in the Interior of Northern Germany.
Hald, M., Korsun, S., 1997. Distribution of modern benthic foraminifera from fjords of Svalbard, European Arctic. J. Foraminifer. Res. 27 (2), 101–122.
Hammer, Ø., Harper, D.A., Ryan, P.D., 2001. PAST: Paleontological statistics software package for education and data analysis. Palaeontol. Electron. 4 (1), 9.
Hammer, Ø., Harper, D., Ryan, P., 2008. PAST—PAlaeontological STatistics, ver. 1.81. Software Documentation.
Hayward, B.W., 2004. Foraminifera-based estimates of paleobathymetry using Modern Analogue Technique, and the subsidence history of the early Miocene Waitemata Basin. N. Z. J. Geol. Geophys. 47 (4), 749–767.
Hayward, B.W., Carter, R., Grenfell, H.R., Hayward, J.J., 2001. Depth distribution of recent deep-sea benthic foraminifera east of New Zealand, and their potential for improving paleobathymetric assessments of Neogene microfaunas. N. Z. J. Geol. Geophys. 44 (4), 555–587.
Hernández-Molina, F., Stow, D., Alvarez-Zarikian, C., Expedition, I., 2013. IODP Expedition 339 in the Gulf of Cadiz and off West Iberia: decoding the environmental significance of the Mediterranean outflow water and its global influence. Sci. Drill. 16, 1–11.
Hernandez-Molina, F.J., Stow, D.A.V., Alvarez-Zarikian, C.A., Acton, G., Bahr, A., Balestra, B., Ducassou, E., Flood, R., Flores, J.A., Furota, S., Grunert, P., Hodell, D., Jimenez-Espejo, F., Kim, J.K., Krissek, L., Kuroda, J., Li, B., Llave, E., Lofi, J., Lourens, L., Miller, M., Nanayama, F., Nishida, N., Richter, C., Roque, C., Pereira, H., Sanchez Goni, M.F., Sierro, F.J., Singh, A.D., Sloss, C., Takashimizu, Y., Tzanova, A., Voelker, A., Williams, T., Xuan, C., 2014. Onset of Mediterranean outflow into the North. Atlantic. 344 (6189), 1244–1250.
Hernández-Molina, F., Sierro, F., Llave, E., Roque, C., Stow, D., Williams, T., Lofi, J., Van der Schee, M., Arnáiz, A., Ledesma, S., 2016. Evolution of the gulf of Cadiz margin and Southwest Portugal contourite depositional system: Tectonic, sedimentary and paleoceanographic implications from IODP expedition 339. Mar. Geol. 377, 7–39.
Hodell, D.A., Curtis, J.H., Sierro, F.J., Raymo, M.E., 2001. Correlation of late Miocene to early Pliocene sequences between the Mediterranean and North Atlantic. Paleoceanography 16 (2), 164–178.
Hohenegger, J., 2005. Estimation of environmental paleogradient values based on presence/absence data: a case study using benthic foraminifera for paleodepth estimation. Palaeogeogr. Palaeoclimatol. Palaeoecol. 217 (1–2), 115–130.
Hohenegger, J., Andersen, N., Baldi, K., Coric, S., Pervesler, P., Rupp, C., Wagreich, M., 2008. Paleoenvironment of the Early Badenian (Middle Miocene) in the southern Vienna Basin (Austria)-multivariate analysis of the Baden-Sooss section. Geol. Carpath. 59 (5), 461–488.
Hsü, K.J., 1972. Origin of saline giants: a critical review after the discovery of the Mediterranean Evaporite. Earth-Sci. Rev. 8 (4), 371–396.
Iaccarino, S., Bossio, A., 1999. Paleoenvironment of uppermost Messinian sequences in the western Mediterranean (Sites 974, 975, and 978). In: Proceedings of the Ocean Drilling Program, Scientific Results, 161, pp. 529–541.
Iaccarino, S., Castradori, D., Cita, M., Di Stefano, E., Gaboardi, S., McKenzie, J., Spezzaferri, S., Sprovieri, R., 1999a. The Miocene/Pliocene boundary and the significance of the earliest Pliocene flooding in the Mediterranean. Mem. Soc. Geol. Ital. 54 (10), 109–131.
Iaccarino, S.M., Cita, M.B., Gaboardi, S., Gruppini, G.M., 1999b. 15. High-Resolution Biostratigraphy at the Miocene/Pliocene boundary in Holes 974b and 975b, Western Mediterranean1. In: Proceedings of the Ocean Drilling Program: Scientific results, pp. 161–197.
Jansen, E., Raymo, M.E., Blum, P., 1996. Leg 162: new frontiers on past climates. Proceedings ODP, Initial Reports 1, 5–20.
Jöhnck, J., Holbourn, A., Kuhnt, W., Andersen, N., 2021. Oxygen isotope offsets in deep-water benthic foraminifera. J. Foraminifer. Res. 51 (3), 225–244.
Jorissen, F.J., 1987. The distribution of benthic foraminifera in the Adriatic Sea. Mar. Micropaleontol. 12, 21–48.
Jorissen, F.J., 1999. Benthic foraminiferal successions across Late Quaternary Mediterranean sapropels. Mar. Geol. 153 (1–4), 91–101.
Jorissen, F.J., 1999. Benthic foraminiferal successions across Late Quaternary Mediterranean sapropels. Mar. Geol. 153 (1–4), 91–101.
Jorissen, F.J., de Stigter, H.C., Widmark, J.G., 1995. A conceptual model explaining benthic foraminiferal microhabitats. Mar. Micropaleontol. 26 (1–4), 3–15.
Jorissen, F., Fontanier, C., Thomas, E., 2007. Paleoceanographical Proxies based on Deep-Sea Benthic Foraminiferal Assemblage Characteristics, 1 (07). https://doi.org/10.1016/S1572-5480(07):01012-3.
Kaboth, S., de Boer, B., Bahr, A., Zeeden, C., Lourens, L.J., 2017. Mediterranean Outflow Water dynamics during the past∼ 570 kyr: regional and global implications. Paleoceanography 32 (6), 634–647.
Kaiho, K., 1991. Global changes of Paleogene aerobic/anaerobic benthic foraminifera and deep-sea circulation. Palaeogeogr. Palaeoclimatol. Palaeoecol. 83 (1–3), 65–85.
Kaiho, K., 1994. Benthic foraminiferal dissolved-oxygen index and dissolved-oxygen levels in the modern ocean. Geology 22 (8), 719–722.
Kaiho, K., 1999. Effect of organic carbon flux and dissolved oxygen on the benthic foraminiferal oxygen index (BFOI). Mar. Micropaleontol. 37 (1), 67–76.
Kaminski, M.A., 2012. Calibration of the benthic foraminiferal oxygen index in the Marmara Sea. Geol. Quart. 56 (4), 757–764. https://doi.org/10.7306/gq. 1061.
Karakitsios, V., Roveri, M., Lugli, S., Manzi, V., Gennari, G., Antonarakou, A., Triantaphyllou, M., Agiadi, K., Kontakiotis, G., Kafousia, N., de Rafelis, M., 2017. A record of the Messinian salinity crisis in the eastern Ionian tectonically active domain (Greece, eastern Mediterranean). Bas. Res. 29, 203–233. https://doi.org/10.1111/bre.12173.
Koho, K., García, R.d., De Stigter, H., Epping, E., Koning, E., Kouwenhoven, T., Van der Zwaan, G., 2008. Sedimentary labile organic carbon and pore water redox control on species distribution of benthic foraminifera: a case study from Lisbon–Setúbal Canyon (southern Portugal). Prog. Oceanogr. 79 (1), 55–82.
Kontakiotis, G., Karakitsios, V., Mortyn, P., Antonarakou, A., Drinia, H., Anastasakis, G., Agiadi, K., Kafousia, N., De Rafelis, M., 2016. New insights into the early Pliocene hydrographic dynamics and their relationship to the climatic evolution of the Mediterranean Sea. Palaeogeogr. Palaeoclimatol. Palaeoecol. 459, 348–364.
Krijgsman, W., Stoica, M., Vasiliev, I., Popov, V.V., 2010. Rise and fall of the Paratethys Sea during the Messinian Salinity Crisis. 290 (1–2), 183–191.
Kucera, M., 2007. Planktonic foraminifera as tracers of past oceanic environments. In: Developments in marine geology, Chapter 6, pp. 213–262.
Langezaal, A., Jorissen, F., Braun, B., Chaillou, G., Fontanier, C., Anschutz, P., Van der Zwaan, G., 2006. The influence of seasonal processes on geochemical profiles and foraminiferal assemblages on the outer shelf of the Bay of Biscay. Cont. Shelf Res. 26 (15), 1730–1755.
Laube-Lenfant, E., Pierre, C., 1994. Variability of delta-c-13 of sigma-co2 in ocean waters of the equatorial pacific. Oceanol. Acta 17 (6), 633–641.
Licari, L., Mackensen, A., 2005. Benthic foraminifera off West Africa (1° N to 32° S): do live assemblages from the topmost sediment reliably record environmental variability? Mar. Micropaleontol. 55 (3–4), 205–233.
Loget, N., Van Den Driessche, J., 2006. On the origin of the Strait of Gibraltar. Sediment. Geol. 188, 341–356.
Loget, N., Driessche, J.V.D., Davy, P., 2005. How did the Messinian salinity crisis end? Terra Nova 17 (5), 414–419.
Loubère, P., Banonis, G., Jakiel, R., 1988. Globocassidulina subglobosa (Brady); environmental control of species abundance and specimen test size. J. Foraminifer. Res. 18 (1), 6–15.
Lutze, G., Coulbourn, W., 1984. Recent benthic foraminifera from the continental margin of Northwest Africa: community structure and distribution. Mar. Micropaleontol. 8 (5), 361–401.
Lutze, G.F., Wefer, G., 1980. Habitat and asexual reproduction of Cyclorbicula compressa (Orbigny), Soritidae. J. Foraminifer. Res. 10 (4), 251–260.
Madof, A.S., Bertoni, C., Lofi, J., 2019. Discovery of vast fluvial deposits provides evidence for drawdown during the late Miocene Messinian salinity crisis. Geology 47 (2), 171–174.
Manzi, V., Roveri, M., 2009. The Terminal Carbonate Complex: the record of sea-level changes during the Messinian salinity crisis. GeoActa 8, 63–77.
Manzi, V., Lugli, S., Roveri, M., Dela Pierre, F., Gennari, R., Lozar, F., Natalicchio, M., Schreiber, B.C., Taviani, M., Turco, E., 2016. The Messinian salinity crisis in Cyprus: a further step towards a new stratigraphic framework for Eastern Mediterranean. Basin Res. 28 (2), 207–236.
Martín, J.M., Puga-Bernabéu, A., Aguirre, J., Braga, J.C., 2014. Miocene Atlantic-Mediterranean seaways in the Betic Cordillera (Southern Spain). Rev. Soc. Geol. Esp. 27 (1), 175–186.
Marzocchi, A., Flecker, R., Van Baak, C.G., Lunt, D.J., Krijgsman, W., 2016. Mediterranean outflow pump: an alternative mechanism for the Lago-mare and the end of the Messinian Salinity Crisis. Geology 44 (7), 523–526.
Mather, A.E., Stokes, M., 2001. Marine to Continental Transition. A Field Guide to the Neogene Sedimentary Basins of the Almería Province, SE Spain, pp. 186–224.
McKenzie, J.A., Sprovieri, R., Channell, J., 1990. The terminal Messinian flood and earliest Pliocene paleoceanography in the Mediterranean: results from ODP Leg 107, Site 652, Tyrrhenian Sea. Mem. Soc. Geol. Ital. 44, 81–91.

MEDARGroup, 2002. Medatlas 2002: Mediterranean and Black Sea Database of Temper-Ature, Salinity and Biochemical Parameters—Climatological Atlas. IFREMER, Brest, France.
Mendes, I., Gonzalez, R., Dias, J., Lobo, F., Martins, V., 2004. Factors influencing recent benthic foraminifera distribution on the Guadiana shelf (Southwestern Iberia). Mar. Micropaleontol. 51 (1–2), 171–192.
Mendes, I., Dias, J.A., Schönfeld, J., Ferreira, Ó., 2012. Distribution of living benthic foraminifera on the northern Gulf of Cadiz continental shelf. J. Foraminifer. Res. 42 (1), 18–38.
Miao, Q., Thunell, R.C., 1993. Recent deep-sea benthic foraminiferal distributions in the South China and Sulu Seas. Mar. Micropaleontol. 22 (1–2), 1–32.
Milker, Y., 2010. Western Mediterranean Shelf Foraminifera: Recent Distribution, Holocene Sea-Level Reconstructions, and Paleoceanographic Implications.
Milker, Y., Schmiedl, G., 2012. A taxonomic guide to modern benthic shelf foraminifera of the western Mediterranean Sea. Palaeontol. Electron. 15 (2), 1–134.
Milker, Y., Weinkauf, M.F., Titschack, J., Freiwald, A., Krüger, S., Jorissen, F.J., Schmiedl, G., 2017. Testing the applicability of a benthic foraminiferal-based transfer function for the reconstruction of paleowater depth changes in Rhodes (Greece) during the early Pleistocene. PLoS One 12 (11), e0188447.
Mojtahid, M., Jorissen, F., Durrieu, J., Galgani, F., Howa, H., Redois, F., Camps, R., 2006. Benthic foraminifera as bio-indicators of drill cutting disposal in tropical East Atlantic outer shelf environments. Mar. Micropaleontol. 61 (1–3), 58–75.
Morigi, C., Jorissen, F., Gervais, A., Guichard, S., Borsetti, A., 2001. Benthic foraminiferal faunas in surface sediments off NW Africa: relationship with organic flux to the ocean floor. J. Foraminifer. Res. 31 (4), 350–368.
Murray, J., 1991. Ecology and Palaeoecology of Benthic Foraminifera: Longman Scientific and Technical. Harlow, Essex, UK.
Murray, J.W., 2001. The niche of benthic foraminifera, critical thresholds and proxies. Mar. Micropaleontol. 41 (1–2), 1–7.
Murray, J.W., 2006. Ecology and Applications of Benthic Foraminifera. Cambridge University Press.
Naeher, S., Geraga, M., Papatheodorou, G., Ferentinos, G., Kaberi, H., Schubert, C.J., 2012. Environmental variations in a semi-enclosed embayment (Amvrakikos Gulf, Greece)–reconstructions based on benthic foraminifera abundance and lipid biomarker pattern. Biogeosciences 9 (12), 5081–5094.
Ochoa, J., Bray, N., 1991. Water mass exchange in the Gulf of Cadiz. Deep Sea Research Part A. Oceanogr. Res. Papers 38, S465–S503.
Ohga, T., Kitazato, H., 1997. Seasonal changes in bathyal foraminiferal populations in response to the flux of organic matter (Sagami Bay, Japan). Terra Nova 9 (1), 33–37.
Omodeo Salé, S., Gennari, R., Lugli, S., Manzi, V., Roveri, M., 2012. Tectonic and climatic control on the late Messinian sedimentary evolution of the Nijar Basin (Betic Cordillera, Southern Spain). Basin Res. 24 (3), 314–337.
Orszag-Sperber, F., 2006. Changing perspectives in the concept of "Lago-Mare" in Mediterranean late Miocene evolution. Sediment. Geol. 188, 259–277.
Pérez-Asensio, J.N., Aguirre, J., Schmiedl, G., Civis, J., 2012. Messinian paleoenvironmental evolution in the lower Guadalquivir Basin (SW Spain) based on benthic foraminifera. Palaeogeogr. Palaeoclimatol. Palaeoecol. 326, 135–151.
Pérez-Asensio, J.N., Aguirre, J., Jiménez-Moreno, G., Schmiedl, G., Civis, J., 2013. Glacioeustatic control on the origin and cessation of the Messinian salinity crisis. Glob. Planet. Chang. 111, 1–8.
Pérez-Asensio, J.N., Frigola, J., Pena, L.D., Sierro, F.J., Reguera, M.I., Rodríguez-Tovar, F.J., Dorador, J., Asioli, A., Kuhlmann, J., Huhn, K., 2020. Changes in western Mediterranean thermohaline circulation in association with a deglacial Organic Rich Layer formation in the Alboran Sea. Quat. Sci. Rev. 228, 106075.
Pérez-Asensio, J.N., Rodríguez-Tovar, F.J., Łaska, W., Uchman, A., 2021. Palaeoenvironmental changes after the Messinian Salinity Crisis in the Mediterranean Almería-Níjar Basin (SE Spain) recorded by benthic foraminifera. Palaeogeogr. Palaeoclimatol. Palaeoecol. 110536.
Pflum, C.E., Frerichs, W.E., Sliter, W.V., 1976. Gulf of Mexico Deep-Water Foraminifers. Cushman Foundation for Foraminiferal Research, p. 14.
Pierre, C., 1999. The oxygen and carbon isotope distribution in the Mediterranean water masses. Mar. Geol. 153 (1–4), 41–55.
Pierre, C., Caruso, A., Blanc-Valleron, M.-M., Rouchy, J.M., Orzsag-Sperber, F., 2006. Reconstruction of the paleoenvironmental changes around the Miocene–Pliocene boundary along a West–East transect across the Mediterranean, 188-189, pp. 319–340.
Platon, E., Gupta, B.K.S., Rabalais, N.N., Turner, R.E., 2005. Effect of seasonal hypoxia on the benthic foraminiferal community of the Louisiana inner continental shelf: the 20th century record. Mar. Micropaleontol. 54 (3–4), 263–283.
Poag, C.W., Tresslar, R.C., 1981. Living foraminifers of West Flower Garden Bank, northernmost coral reef in the Gulf of Mexico. Micropaleontology 27 (1), 31–62.
Radionova, E.P., Golovina, L.A., Filippova, N.Y., Trubikhin, V.M., Popov, S.V., Goncharova, I.A., Vernigorova, Y.V., Pinchuk, T.N., 2012. Middle-Upper Miocene stratigraphy of the Taman Peninsula, Eastern Paratethys. Central Eur. J. Geosci. 4 (1), 188–204.
Raymo, M.E., Kozdon, R., Evans, D., Lisiecki, L., Ford, H.L., 2018. The accuracy of mid-Pliocene δ18O-based ice volume and sea level reconstructions. Earth Sci. Rev. 177, 291–302.
Riforgiato, F., Foresi, L.M., Di Stefano, A., Aldinucci, M., Pelosi, N., Mazzei, R., Salvatorini, G., Sandrelli, F., 2011. The Miocene/Pliocene boundary in the Mediterranean area: New insights from a high-resolution micropalaeontological and cyclostratigraphical study (Cava Serredi section, Central Italy). 305 (1–4), 310–328.
Rohling, E., Marino, G., Grant, K., 2015. Mediterranean climate and oceanography, and the periodic development of anoxic events (sapropels). Earth Sci. Rev. 143, 62–97.
Ross, D.A., Degens, E.T., 1974. Recent Sediments of Black Sea: Sediments.
Rouchy, J.M., Caruso, A., 2006. The Messinian salinity crisis in the Mediterranean basin: a reassessment of the data and an integrated scenario. Sediment. Geol. 188-189, 35–67.
Rouchy, J., Orszag-Sperber, F., Blanc-Valleron, M.-M., Pierre, C., Rivière, M., Combourieu-Nebout, N., Panayides, I., 2001. Paleoenvironmental changes at the Messinian–Pliocene boundary in the eastern Mediterranean (southern Cyprus basins): significance of the Messinian Lago-Mare. Sediment. Geol. 145 (1–2), 93–117.
Rouchy, J.M., Caruso, A., Pierre, C., Blanc-Valleron, M.-M., Bassetti, M.A., 2007. The end of the Messinian salinity crisis: evidences from the Chelif Basin (Algeria). Palaeogeogr. Palaeoclimatol. Palaeoecol. 254 (3–4), 386–417.
Roveri, M., Manzi, V., 2006. The Messinian salinity crisis: looking for a new paradigm? Palaeogeogr. Palaeoclimatol. Palaeoecol. 238 (1–4), 386–398.
Roveri, M., Lugli, S., Manzi, V., Schreiber, B.C., 2008. The Messinian Sicilian stratigraphy revisited: new insights for the Messinian salinity crisis. Terra Nova 20 (6), 483–488.
Roveri, M., Flecker, R., Krijgsman, W., Lofi, J., Lugli, S., Manzi, V., Sierro, F.J., Bertini, A., Camerlenghi, A., De Lange, G., 2014a. The Messinian Salinity Crisis: past and future of a great challenge for marine sciences. Mar. Geol. 352, 25–58.
Roveri, M., Manzi, V., Bergamasco, A., Falcieri, F.M., Gennari, R., Lugli, S., Schreiber, B. C., 2014b. Dense shelf water cascading and messinian canyons: a new scenario for the mediterranean salinity crisis. Am. J. Sci. 314 (3), 751–784.
Roveri, M., Gennari, R., Persico, D., Rossi, F.P., Lugli, S., Manzi, V., Reghizzi, M., Taviani, M., 2018. A new chronostratigraphic and palaeoenvironmental framework for the end of the Messinian salinity crisis in the Sorbas Basin (Betic Cordillera, southern Spain). Geol. J. 54, 1617–1637.
Roveri, M., Gennari, R., Ligi, M., Lugli, S., Manzi, V., Reghizzi, M., 2019a. The synthetic seismic expression of the Messinian salinity crisis from onshore records: implications for shallow-to deep-water correlations. Basin Res. 31 (6), 1121–1152.
Roveri, M., Gennari, R., Persico, D., Rossi, F.P., Lugli, S., Manzi, V., Reghizzi, M., Taviani, M., 2019b. A new chronostratigraphic and palaeoenvironmental framework for the end of the Messinian salinity crisis in the Sorbas Basin (Betic Cordillera, southern Spain). Geol. J. 54 (3), 1617–1637.
Russo, B., Curcio, E., Iaccarino, S., 2007. Paleoecology and paleoceanography of a Langhian succession (Tremiti Islands, southern Adriatic Sea, Italy) based on benthic foraminifera. Bol. Soc. Paleontol. Ital. 46, 107–124.
Sant, K., Palcu, D., Turco, E., Di Stefano, A., Baldassini, N., Kouwenhoven, T., Kuiper, K., Krijgsman, W., 2019. The mid-Langhian flooding in the eastern Central Paratethys: integrated stratigraphic data from the Transylvanian Basin and SE Carpathian Foredeep. Int. J. Earth Sci. 108 (7), 2209–2232.
Sanz De Galdeano, C., Vera, J.A., 1992. Stratigraphic record and palaeogeographical context of the Neogene basins in the Betic Cordillera, Spain. Basin Res. 4 (1), 21–36.
Schmiedl, G., Mackensen, A., Müller, P., 1997. Recent benthic foraminifera from the eastern South Atlantic Ocean: dependence on food supply and water masses. Mar. Micropaleontol. 32 (3–4), 249–287.
Schmiedl, G., De Bovée, F., Buscail, R., Charriere, B., Hemleben, C., Medernach, L., Picon, P., 2000. Trophic control of benthic foraminiferal abundance and microhabitat in the bathyal Gulf of Lions, western Mediterranean Sea. Mar. Micropaleontol. 40 (3), 167–188.
Schmiedl, G., Mitschele, A., Beck, S., Emeis, K.-C., Hemleben, C., Schulz, H., Sperling, M., Weldeab, S., 2003. Benthic foraminiferal record of ecosystem variability in the eastern Mediterranean Sea during times of sapropel S5 and S6 deposition. Palaeogeogr. Palaeoclimatol. Palaeoecol. 190, 139–164.
Schmiedl, G., Kuhnt, T., Ehrmann, W., Emeis, K.-C., Hamann, Y., Kotthoff, U., Dulski, P., Pross, J., 2010. Climatic forcing of eastern Mediterranean deep-water formation and benthic ecosystems during the past 22 000 years. Quat. Sci. Rev. 29 (23–24), 3006–3020.
Schnitker, D., 1993. Ecostratigraphy of Plio-Pleistocene benthic foraminifers in ODP Hole 625B and four Eureka holes from the Gulf of Mexico. Micropaleontology 404–418.
Schoorl, J., Veldkamp, A., 2003. Late Cenozoic landscape development and its tectonic implications for the Guadalhorce valley near Alora (Southern Spain). Geomorphology 50 (1–3), 43–57.
Schrader, H.-J., 1978. Quaternary through Neogene History of the Black Sea, Deduced from the Paleocology of Diatoms, Silicoflagellates, Ebridians and Chrysomonads.
Sen Gupta, B.K., Machain-Castillo, M.L., 1993. Benthic foraminifera in oxygen-poor habitats 20 (3–4), 183–201.
Serrano, F., 1990. El Mioceno medio en la area de Nijar (Almeria, España). Rev. Soc. Geo. Esp. 3, 1–2.
Sgarrella, F., Sprovieri, R., Di Stefano, E., Caruso, A., 1997. Paleoceanographic conditions at the base of the Pliocene in the Southern Mediterranean Basin. Riv. Ital. Paleontol. Stratigr. 103 (2).
Sharafi, M., Rodríguez-Tovar, F.J., Janočko, J., Bayet-Goll, A., Mohammadi, M., Khanehbad, M., 2021. Environmental significance of trace fossil assemblages in a tide–wave-dominated shallow-marine carbonate system (Lower Cretaceous), northern Neo-Tethys margin, Kopet-Dagh Basin, Iran. Int. J. Earth Sci. 1–24.
Sierro, F.J., Flores, J.A., Civis, J., González Delgado, J.A., Francés, G., 1993. Late Miocene globorotaliid event-stratigraphy and biogeography in the NE-Atlantic and Mediterranean. Mar. Micropaleontol. 21 (1–3), 143–167.
Singh, A., Rai, A., Tiwari, M., Naidu, P., Verma, K., Chaturvedi, M., Niyogi, A., Pandey, D., 2015. Fluctuations of Mediterranean Outflow Water circulation in the Gulf of Cadiz during MIS 5 to 7: evidence from benthic foraminiferal assemblage and stable isotope records. Glob. Planet. Chang. 133, 125–140.
Smart, C.W., King, S.C., Gooday, A.J., Murray, J.W., Thomas, E., 1994. A benthic foraminiferal proxy of pulsed organic matter paleofluxes. 23 (2), 89–99.

Soria, J., Caracuel, J., Yébenes, A., Fernández, J., Viseras, C., 2005. The stratigraphic record of the Messinian salinity crisis in the northern margin of the Bajo Segura Basin (SE Spain). Sediment. Geol. 179 (3–4), 225–247.
Spellerberg, I.F., Fedor, P.J., 2003. A tribute to Claude Shannon (1916–2001) and a plea for more rigorous use of species richness, species diversity and the 'Shannon–Wiener'Index. Glob. Ecol. Biogeogr. 12 (3), 177–179.
Sprovieri, R., Hasegawa, S., 1990. Plio-Pleistocene Benthic Foraminifer Stratigraphic Distribution in the Deep-Sea Record of the Tyrrhenian Sea (ODP Leg 107), Proceedings of the Ocean Drilling Program. Scientific Results. Ocean Drilling Program College Station, TX, pp. 429–459.
Stoica, M., Krijgsman, W., Fortuin, A., Gliozzi, E., 2016. Paratethyan ostracods in the Spanish Lago-Mare: more evidence for interbasinal exchange at high Mediterranean sea level. Palaeogeogr. Palaeoclimatol. Palaeoecol. 441, 854–870.
Suokhrie, T., Saraswat, R., Nigam, R., 2021. Multiple ecological parameters affect living Benthic Foraminifera in the river-influenced west-central Bay of Bengal. Front. Mar. Sci. 8, 467.
Theodor, M., Schmiedl, G., Jorissen, F., Mackensen, A., 2016a. Stable carbon isotope gradients in benthic foraminifera as proxy for organic carbon fluxes in the Mediterranean Sea. Biogeosciences 13 (23), 6385–6404.
Theodor, M., Schmiedl, G., Mackensen, A., 2016b. Stable isotope composition of deep-sea benthic foraminifera under contrasting trophic conditions in the western Mediterranean Sea. Mar. Micropaleontol. 124, 16–28.
Trenkwalder, S., Violanti, D., d'Atri, A., Lozar, F., Dela Pierre, F., Irace, A., 2008. The Miocene/Pliocene boundary and the early Pliocene micropalaeontological record: new data from the Tertiary Piedmont Basin (Moncucco Quarry, Torino Hill, Northwestern Italy). Bol. Soc. Paleontol. Ital. 47 (2), 87–103.
Tulbure, M., Capella, W., Barhoun, N., Flores, J., Hilgen, F., Krijgsman, W., Kouwenhoven, T., Sierro, F.J., Yousfi, M.Z., 2017. Age refinement and basin evolution of the North Rifian Corridor (Morocco): no evidence for a marine connection during the Messinian Salinity Crisis. Palaeogeogr. Palaeoclimatol. Palaeoecol. 485, 416–432.
Uchman, A., Demircan, H., 1999. Trace fossils of Miocene deep-sea fan fringe deposits from the Cingöz Formation, southern Turkey. Ann. Soc. Geol. Pol. 125–135.
Van Der Schee, M., Sierro, F.J., Jiménez-Espejo, F.J., Hernández-Molina, F.J., Flecker, R., Flores, J.A., Acton, G., Gutjahr, M., Grunert, P., García-Gallardo, Á., Andersen, N., 2016. Evidence of early bottom water current flow after the Messinian Salinity Crisis in the Gulf of Cadiz. 380, 315–329.
Van der Zwaan, G.J., 1982. Paleoecology of Late Miocene Mediterranean Foraminifera. Utrecht University.
Van der Zwaan, G., Jorissen, F., De Stigter, H., 1990. The depth dependency of planktonic/benthic foraminiferal ratios: constraints and applications. Mar. Geol. 95 (1), 1–16.
Van der Zwaan, G., Duijnstee, I., Den Dulk, M., Ernst, S., Jannink, N., Kouwenhoven, T., 1999. Benthic foraminifers: proxies or problems?: a review of paleocological concepts. Earth Sci. Rev. 46 (1–4), 213–236.
Van Hinsbergen, D.J.J., Kouwenhoven, T.J., Van Der Zwaan, G.J., 2005. Paleobathymetry in the backstripping procedure: Correction for oxygenation effects on depth estimates. 221 (3–4), 245–265.
Van Morkhoven, F.M., Berggren, W.A., Edwards, A.S., 1986. Cenozoic cosmopolitan deep-water benthic foraminifera. Bull. Centres Rech. Explorat. Prod. 11 (elf-aquitaine(11).
Van Rooij, D., De Mol, L., Le Guilloux, E., Wisshak, M., Huvenne, V., Moeremans, R., Henriet, J.-P., 2010. Environmental setting of deep-water oysters in the Bay of Biscay. Deep-Sea Res. I Oceanogr. Res. Pap. 57 (12), 1561–1572.
Venz, K.A., Hodell, D.A., Stanton, C., Warnke, D.A., 1999. A 1.0 Myr record of Glacial North Atlantic Intermediate Water variability from ODP site 982 in the northeast Atlantic. Paleoceanography 14 (1), 42–52.
Verhallen, P.J., 1991. Late Pliocene to Early Pleistocene Mediterranean Mud-Dwelling Foraminifera: Influence of a Changing Environment on Community Structure and Evolution. Utrecht University.
Violanti, D., Trenkwalder, S., Lozar, F., Gallo, L.M., 2009. Micropalaeontological analyses of the Narzole core: biostratigraphy and palaeoenvironment of the late Messinian and early Zanclean of Piedmont (Northwestern Italy). Bol. Soc. Paleontol. Ital. 48 (3), 167–181.
Violanti, D., Dela Pierre, F., Trenkwalder, S., Lozar, F., Clari, P., Irace, A., D'Atri, A., 2011. Biostratigraphic and palaeoenvironmental analyses of the Messinian/Zanclean boundary and Zanclean succession in the Moncucco quarry (Piedmont, northwestern Italy). Bull. Soc. Géol. France 182 (2), 149–162.
Wright, R., 1978. 41. Neogene paleobathymetry of the Mediterranean based on benthic foraminifers from DSDP Leg 42a. Initial Reports DSDP 42, 837–847.
Wright, R., 1979. Benthic foraminiferal repopulation of the Mediterranean after the Messinian (late Miocene) event. Palaeogeogr. Palaeoclimatol. Palaeoecol. 29, 189–214.